# Use Of Radiation Absorbing Gaseous Media In Flat Plate Solar Collectors

by

SARVESH PARIMAL VATSA

DEPARTMENT OF MECHANICAL ENGINEERING

INDIAN INSTITUTE OF TECHNOLOGY KANPUR

MAY, 1995

Use Of Radiation Absorbing Gaseous Media In Flat Plate Solar Collectors

A Dissertation Submitted
in Partial Fulfillment of the Requirements
for the Degree of
MASTER OF TECHNOLOGY

By

SARVESH PARIMAL VATSA

To the

Department of Mechanical Engineering
Indian Institute of Technology, Kanpur – 208 016. INDIA
May,1995

CERTIFICATE

It is certified that the work contained in this thesis titled *Use Of Radiation Absorbing Gaseous Media In Flat Plate Solar Collectors* by Sarvesh Parimal Vatsa has been carried under my supervision and this work has not been submitted elsewhere for the award of a degree.
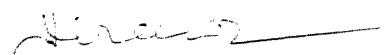
Dr. Manohar Prasad

Professor

Department of Mechanical Engineering,

Indian Institute Of Technology,

Kanpur.

ABSTRACT

The feasibility of using radiation absorbing gaseous media is analyzed theoretically and experimentally verified. The radiation absorbing gaseous media like CO_2 and NH_3 tend to reduce the thermal radiation falling on the inner side of the glass cover, from the absorber plates by absorbing it when it passes through it. (But these gases are nearly transparent for solar radiation.) Simultaneously the gaseous medium emits thermal radiation uniformly in all directions increasing the thermal radiation falling on the inner side of the glass cover. But the temperature of the gas being lower than that of the absorber plate, and the thermal absorptivity and emissivity of the gas being approximately equal, results in the net reduction in the total thermal radiation falling on the inner side of the glass cover. This reduced thermal radiation on the glass sheet causes lowering of the outer cover temperature, which reduces the convective and radiative heat losses from the outer side of the glass cover. In the present theoretical work, a specific type of solar collector has been designed and the heat collection efficiency at various outlet temperatures is calculated for collector and gaps with air, with gaseous media and with vacuum. For simplicity of the computations, walls are assumed to be gray, highly absorbing and emitting and gaseous media to be isothermal, this enables to use the Hottel's emissivity charts.

Acknowledgements

I express my heartful thanks to my thesis supervisor Dr. Manohar Prasad for his valuable guidance and constant encouragement throughout the thesis work. I am extremely grateful to him for his being very accommodating and understanding. During my thesis work, many times the situation of complete hopelessness arrived, but it was his patience that he allowed me to continue the work and to achieve the results.

I thank Mr. S. N. Sharma for his cooperation in the fabrication of the experimental set-up.

I thank Mr. S. Mishra for his cooperation in the testing of the experimental set-up.

Lastly, I would like to thank each and everybody whoever have motivated me directly or indirectly, during my thesis work.

<div align="right">Sarvesh Parimal Vatsa</div>

Contents

List of Tables

List of Figures

Nomenclature

Notation	Explanation
A_b	Base area
γ	Extinction coefficient
n	Refractive index
W_B	Black body emissive power
σ	Stefan Boltzman constant
ω	Solid angle
J_λ	Spectral volume emissive power
ΔE	Emission from the ith strip of the glass sheet
T_g	Temperature of glass sheet
$T_{ig,i}$	Temperature of ith wall of ig^{th} gap
$T_{B,i}$	Temperature of ith wall of Box
θ_h	Angle of sun rays from horizontal plane
θ_i	Angle of sun rays from vertical plane
β	Inclination of collector from local horizontal plane
Q_r^{up}	Primary emission from all strips in upper direction
Q_r^{lp}	Primary emission from all strips in lower direction
$Q_{in_{j,r}}^{sb}$	Solar energy falling on right wall of jth gap
$Q_{in_{j,l}}^{sb}$	Solar energy falling on left wall of jth gap
$Q_{in_{j,b}}^{sb}$	Solar energy falling on j^{th} glass cover
$Q_{in_{B,r}}^{sb}$	Solar energy falling on right wall of box
$Q_{in_{B,l}}^{sb}$	Solar energy falling on left wall of box
$Q_{in_{B,b}}^{sb}$	Solar energy falling on Base of box
N_{cover}	Number of glass sheets
N_x	Number of division of glass sheet into strips
N_θ	Number of division in θ direction for numerical integration
L_a, L_b, L_c	Length, width and height of the Box respectively
L^m	Geometric Mean Beam Length
Δg	Glass sheet thickness
Δ_{gap}	Size of gap between two glass sheets

Symbol	Description
τ_g	Transmissivity of glass sheet
ρ_g	Reflectivity of glass sheet
α_g	Absorptivity of glass sheet
pL	Partial pressure of mixture
$\tau_{ig,ij}^{mix}$	Transmissivity of gas in ig^{th} gap from wall i to j
$\epsilon_{ig,j}$	Emissivity of jth wall of ig^{th} gap
$\tau_{B,ij}^{mix}$	Transmissivity of gas in Box from wall i to j
$G_{ig,j}^{th}$	Thermal irradiation on j^{th} wall of ig^{th} gap
$G_{ig,j}^{so}$	Solar irradiation on j^{th} wall of ig^{th} gap
$G_{B,j}^{th}$	Thermal irradiation on j^{th} wall of Box
$G_{B,j}^{so}$	Solar irradiation on j^{th} wall of Box
$\alpha_{ig,j}$	Absorptivity of jth wall of ig^{th} gap
$\alpha_{B,j}$	Absorptivity of jth wall of Box
$\epsilon_{ig,j}$	Emissivity of jth wall of ig^{th} gap
$\epsilon_{B,j}$	Emissivity of jth wall of Box
F_{ij}	Shape factor between ij for Box
$F_{ig,ij}$	Shape factor between ij for ig^{th} gap
h	Heat transfer coefficient
Cp	Specific heat of material denoted by subscripts
L_{ch}	Side of the channel
ρ_f	Density of heat collecting fluid
T_{p_i}, T_{p_o}	Wall temperature of inside and side facing solar energy
T_{f_i}, T_{f_o}	Heat collecting Fluid temperature at inlet and outlet of channel
A_{ch}	Area of wall in contact with the channel
V_f	Velocity of heat collecting fluid in channel
V_{air}	Wind Velocity at outer cover surface
Δ_p	Plate thickness
K_p, K_f	Thermal conductivity of plate and heat collecting fluid
Pr	Prandtl no. of the fluid denoted by subscript
D_{eq}	Hydrolic diameter of the channel
R_{e_D}	Reynolds no. based on diameter

$frac_1$	Fraction of total upward primary radiation emerging as emission from upper surfac
$frac_2$	Fraction of total upward primary radiation emerging as emission from upper surfac
Q_r^u, Q_r^l	Total emission from glass sheet in upper and lower directions
$Q_{abs_j}^p$	Total Primary energy absorbed in j^{th} strip
$Q_{abs_j}^s$	Total secondary energy absorbed in j^{th} strip
$Q_{d_j}^{sb}$	Amount of beam solar radiation absorbed in j^{th} strip
$Q_{cv_{ig}}^l$	Convective heat transfer from the lower side of ig^{th} glass sheet
$Q_{cv_{ig}}^u$	Convective heat transfer from the upper side of ig^{th} glass sheet
Q_{sky}	Diffuse sky radiation exchange between collector surface and sky
Q_{in}^{sd}	Total diffuse solar radiation falling on outer cover
δs	Solar declination angle
a_s	Solar azimuth angle
a_c	Surface azimuth angle
α	Solar altitude angle
H_s	Solar hour angle
L	Lattitude angle of the cite
N_{day}	Number of the day 1 for January 1st
I_{sc}	Solar constant
I_o	Extraterrestrial solar radiation intensity
I_{oh}	Extraterrestrial horizontal solar radiation intensity
I_h	Terrestrial horizontal solar radiation intensity
I_b	Terrestrial beam solar radiation intensity
I_{bc}	Terrestrial beam solar radiation intensity on collector surface
I_{dc}	Terrestrial diffuse solar radiation intensity on collector surface
K_T	Clearness index or atmospheric transmittance

Super-scripts :

sb	for Beam solar radiation
sd	for Diffuse solar radiation
th	for Thermal radiation
in	for Infrared radiation
so	for solar radiation without distinguishing the nature
mix	for gas mixture

Sub-scripts :

T	from Top
L	from Bottom
b	for Base
l	for Left Wall
r	for Right Wall
ch	for Channel
g	for Glass
B	for Box, space between absorber plates and glass cover
in	for input beam solar radiation
cv	for convective heat loss

Chapter 1

Introduction

1.1   Solar energy : Promises and Challenges

- Solar radiation is incident on the earth's surface at the rate of approximately $8 \times 10^{16} W$, which is more than 10000 times the present world energy consumption.

- Our energy use includes several forms of delivered energy, in particular, heating and cooling, light ing, mechanical motion and the industrial production. In most cases the useful energy is different from the input energy form.

  When considering the renewable energy sources, attention must be paid to the best possible match between available energy type and the desired end use energy type. Table 1 shows the conversion efficiency for different solar energy conversion methods.

- From the Table 1 , it is evident that biomass should not be used for heating purpose because the conversion efficiency of the solar to biomass is very low ,

Table 1: Solar Energy Conversion Methods and Typical Annual Average System efficiencies. [14]

System and collector type	Percent efficiency (relative to radiation incident on aperture)	Comments
(i) Heat	30–60	For a given system the efficiency decreases with temperature. Higher temperature collectors tend to cost more.
(a) Low temperature (hot water, space heating, industrial process heat) Flat plates Evacuated tube Parabolic trough		
(b) High temperature (industrial process heat) Parabolic dish Central receiver		
(ii) Electricity		
(a) Photovoltaic Flat plate Concentrating	5–15 15–25	Probably 10% is the minimum needed for commercial success. Photovoltaic systems could be deployed in small modules (e.g. on roofs).
(b) High temperature Central reciever Parabolic dish Point-focus Fresnel lens	10–25	Short term energy storage as heat.
(iii) Biomass	0.1–2	Energy is stored as chemical.

Table 2: Energy Consumption Pattern of USA in 1977 [14].

Total 80.8 (100%)	Transportation 21.2 (26.2%)			
	Residential plus commercial 29.9 (37.0%)	Residential 18.2 (22.5%)	8.7 (10.8%)	Space heat
			2.5 (3.1%)	Hot water
			1.2 (1.5%)	Air conditioning
			2.4 (3.0%)	Refrigerators and freezers
			1.1 (1.4%)	Lights
			2.3 (2.8%)	Other
		Commercial 11.7 (14.5%)	5.2 (6.4%)	Space heat
			2.5 (3.1%)	Air conditioning
			0.26 (0.3%)	Hot water
			2.5 (3.1%)	Lights
			1.2 (1.5%)	Other
	Industrial 29.7 (36.8%)	Process heat 12.0 (16.0%)	1.0 (1.2%)	Below 100°C
			3.8 (4.7%)	100–177°C
			2.9 (3.6%)	177–288°C
			2.6 (3.2%)	288–593°C
			1.0 (1.2%)	593–1090°C
			1.6 (2.0%)	above 1090°C
		Other industrial 16.8 (20.8%)		

of the order of 1% only. where as the conversion efficiency of solar to thermal is about 30% to 60%.

1.2 Energy Consumption Pattern and Scope for Solar Energy Utilization

Table 2 shows the Energy consumption pattern of USA in 1977. It is found that approximately $2.4 - 4.2\%$ energy is used for heating purpose with the temperature requirement below 100 $°C$. which can be easily supplied by the use of simple nontracking solar collectors. The energy required in the range of 100 $°C$ to 177 $°C$ (about 5% of total energy consumption) can be supplied by the nontracking evacuated collectors. Compound Parabolic Concentrator collectors are available that can operate efficiently

upto 300 °C. The total heating requirement, industrial plus residential, accounts for about 30% of the total energy consumption, which can be supplied by solar energy thermal conversion methods.

These numbers suggest a very large potential for the application of active solar collectors. However, one also needs to consider the relation between the demand and the solar availability. The utilization of the solar equipment is best if there is year-round load. The role of co-generation is also to be emphasized, because when converting solar to electrical, most of the energy is wasted.

Table 3 gives a guide line for the use of nonconventional energy resources in the coming future [29]. It lists the appropriate energy supply technology for different end uses.

1.3   Survey of Solar Collector Technology

The most important and the most expensive component of an active solar energy system is the collector. The survey of the solar collectors, summarized in the tabular form is given below in Tables 4, 5 and 6 [14].

The nontracking collectors are the most economical and the best suited for the application of low temperature requirements. Flat plate collectors are the best developed collectors. A promising low-cost lightweight plastic collector has been developed by Andrew and Wilhelm, 1980, for application where the water quality inside the collector is not as critical as for domestic hot water. Among the solar ponds.shallow solar pond and deep or salt-gradient solar pond are entirely different. The shallow water pond consist of a shallow horizontal water bag, insulated by one or more plastic films

ble 3: A Proposed Long term Solar Energy Economy [29]

MAND SECTOR	END USE ENERGY FORM	APPLICATION	PERCENTAGE OF TOTAL ENERGY USE	APPROPRIATE ENERGY SUPPLY TECHNOLOGY
sidential and nmercial	Low temperature thermal energy (· 212 F)	Space heating, water heating, air conditioning	20–25	Passive and active solar systems, district heating systems
	Intermediate temperature thermal energy (212–572 F)			Active solar heating with concentrating solar collectors
		Cooking and drying	5	
	Hydrogen			Solar thermal, thermochemical, or electrolytic generation
	Methane			Biomass
	Electricity	Lighting, appliances, refrigeration	-- 10	Photovoltaic, wind, solar thermal, total energy systems
		Subtotal	· 35	
strial	Intermediate temperature thermal energy (·.572 F)	Industrial and agricultural process heat and steam	7 5	Active solar heating with flat-plate collectors, and tracking solar concentrators
	High temperature (572 F)	Industrial process heat and steam	17.5	Tracking, concentrating solar collector systems
	Hydrogen			Solar thermal, thermochemical, or electrolytic generation
	Electricity	Co-generation, electric drive, electrolytic, and electrochemical processes	10	Solar thermal, photovoltaic, co-generation, wind systems
	Feedstocks	Supply carbon sources to chemical industries	-- 5	Biomass residues and wastes or plantations
		Subtotal	40	
sportation	Electricity	Electric vehicles, electric rail	10–20	Photovoltaic, wind and solar thermal-electric
	Hydrogen	Aircraft fuel, land and water transportation vehicles		Solar thermal, thermochemical, or electrolytic generation
	Liquid fuels methanol, ethanol, gasoline	Long distance land and water transportation vehicles	5-15	Biomass residues and wastes or plantations
		Subtotal	-- 25	
			100	

JRCE: Henry Kendall and Steven Nadis, *Energy Strategies: Toward a Solar Future*, pp. 262–263.

Table 4: Nontracking Collectors

Collector type	Approximate maximum operating temperature (°C)	Cost ($/m²)	Comments
Shallow solar pond	40–60	160[a] (complete system, including storage for 1 day)	Plastic covers may need to be replaced every 5 yr or so. Needs sunny climate for good performance.
Deep solar pond (salt gradient)	40–90	30–60[b] (includes storage)	Collector and longterm storage in one unit. For seasonal storage, depth should be about 3 m. Low cost but low efficiency (10%–20%).
Flat plate			Best known and most developed of all collector types.
(a) Conventional design	40–80	150–300[c,d]	
(b) Made of plastic	30–60	70–100[c,d]	
(c) Unglazed	10–20 above ambient	70–100[c,d]	
Nonevacuated CPC fixed-tilt or summer-to-winter tilt adjustment	80–120	150[c,d]	—
Evacuated tubes (with reflector enhancement; e.g., CPC)	100–200	250–300[c,d]	Many opportunities for cost reduction by mass production and for performance improvements through R&D.

[a]Cost estimate in 1980. Personal communication. Solar Energy Group, Lawrence Livermore Laboratory, Livermore, CA 94550.

[b]Costs of solar ponds are very site-specific (e.g., salt may be free, liner may not be needed, etc.). A 3-m deep salt-gradient solar pond was built in Miamisburg, OH for 35 $/m² in 1978.

[c]*Solar Products Specifications Guide.* 1983. Published annually by *Solar Age Magazine.* Church Hill, Harrisville, NH 03450.

[d]For some collectors several manufacturers are in the market, with a wide spread in quality and price (not always correlated). Some models exceed the price range indicated here.

Table 5: One Axis Tracking Collectors

Collector type	Approximate maximum operating temperature (°C)	Cost (S/m²)	Comments
Inflated cylindrical reflector	140	50–70[a]	Does not need continuous tracking, but does require weekly tilt adjustments; plastic cover may need to be replaced every 5 yr or so.
Parabolic trough	300	150–300[b,c]	Continuous accurate tracking; sensitive to dirt.
Line-focus Fresnel reflector	250	—	May combine advantages of parabolic trough and of central receiver for temperatures below 250°C.
Fixed line-focus reflector with tracking receiver	250	—	Problems with dirt accumulation on reflectors.

[a]Cost estimate in 1980. Personal communication, Solar Energy Group, Lawrence Livermore Laboratory, Livermore, CA 94550.
[b]*Solar Product. Specifications Guide.* 1983. Published annually by *Solar Age Magazine*, Church Hill, Harnsville, NH 03457.
[c]For some collectors several manufacturers are in the market, with a wide spread in quality and price (not always correlated). Some models exceed the price range indicated here.

Table 6: Two Axis Tracking Collectors

Collector type	Approximate maximum operating temperature (°C)	Cost (S/m²)	Comments
Parabolic dish or point-focus Fresnel lens	1500 (possibly more)	—	Good if energy can be used directly in focal zone (e.g., photovoltaics or solar thermal power); otherwise, transporting heat to point of use is problematic.
Central receivers	1000 (possibly more)	492[a] 355[b] plus tower[c]	Optical transport of energy.
Fixed-hemispherical reflector, tracking receiver	400	—	Problems with heat transport to point of use, and with dirt accumulation on reflector.

[a]Average cost of heliostats for Barstow solar power plant in 1980 [Battleson, 1981].

and air layers [Clark and Dickson. 1980]. The deep solar pond uses a thick layer of nonconvecting water as insulation [Tabor and Weinberger. 1980; Neilson. 1980]. Here convection is prevented by adding salt in such a way as to establish a concentration gradient. with a saltier water at the bottom.

Evacuated and concentrating collectors are used to reduce the heat loss. While several attempts have been made to build evacuated flat plates, they do not seem to hold any promise of commercial success. The natural configuration for an evacuated collector is the glass tube. All of the evacuated collectors use selective coating as absorber because with a nonselective absorber. radiation losses would dominate at high temperatures and eliminating convection would not be very effective.

In concentrating collectors, heat losses are reduced by concentrating the radiation incident on the aperture onto a smaller absorber. Presently. the parabolic trough is the favored collector for the temperature range of 150 $°C$ to 300 $°C$. Collectors with a line focus Fresnel lenses pose a problem for large thermal insulation. These collectors have been tested upto 350 $°C$. Attainment of temperatures above 500 $°C$. requires point-focus concentrators. The principal types are the central receivers. the parabolic dish and the point-focus Fresnel lens.

Collectors with high concentration require accurate and continuous tracking and are quite sensitive to dirt accumulation, on both the reflector and the receiver. An interesting alternative to a concentrator with tracking reflector is a fixed reflector with tracking receiver. Last concentrator type is hemispherical fixed reflector with tracking receiver. Like other fixed reflectors it is quite sensitive to dirt accumulation and like the parabolic dish. it faces serious problems of heat transport from absorber to the point of use.
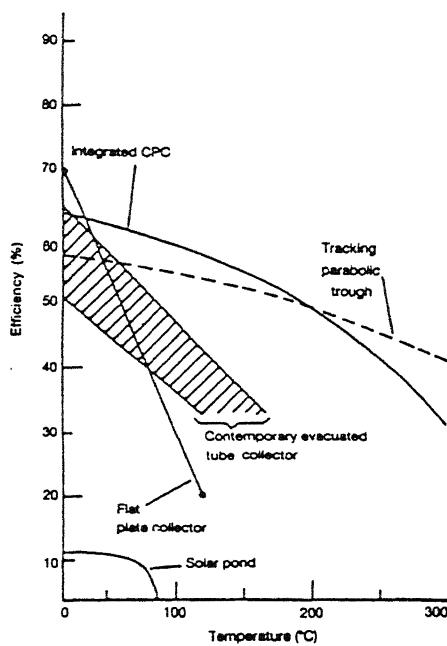
Figure 1: Efficiency and Temperature Range of Various Solar Collectors [31]

The suitable type of solar collector can be selected on the basis of the temperature requirement and the cost of the collector. Figure 1 shows the efficiency and the temperature range of different types of existing solar collectors [31].

Chapter 2

Literature Survey and Present Work

In the light of the present energy crises, people have started thinking seriously in the direction of utilizing non-conventional energy resources and thus extensive work is being done to make the use of these non-conventional energy resources conventional. The use of the solar energy had started a long back, mainly for drying purposes. With the time it extended to the area of water and space heating and then photo-voltaic applications.

2.1   History of Solar Energy Utilization [15]

First instance of the use of solar energy is found in a newspaper of France (Seventeenth century). It states that Archimedes set fire to Marcellus' navy by means of a burning glass composed of small square mirrors moving every way upon hinges which when

placed in the sun's rays, directed them upon the Roman fleet so as to reduce it to ashes at the distance of a bowshot' [15].

For the next 1000 years, most of the devices invented to use solar energy were constructed for amusement purpose. Solar Fountain of de Caus, used several glass lenses to concentrate the sun's rays on an airtight metal chamber partially filled with water. The sun's rays heated the air, thus forcing water out in a small fountain.

The French Scientists George Buffon constructed the first multiple mirror solar furnace in 1747. Lavoisier, was able to melt platinum at 1780 °C, with a special 130 cm. diameter lens filled with alcohal, in the solar furnace.

Pioneering work with flat plate collector was done during the middle of the eighteenth century by the Swiss scientist Nicholes de Saussure. He designed a solar oven consisting of glass plates spaced above a blackened surface enclosed by an insulated box.

A concentrating type of solar cooker was described in an article in Scientific American in 1878 by W. Adams of Bombay, India. Solar cooker that employed parabolic mirror to reach high temperatures and used a means of heat storage enabling food to be cooked after sundown, was developed by Dr. Charles Abbott.

Development of solar powered engines was begun in the latter part of nineteenth century by Augustin Mouchot in France and John Erricsson in the United States. A water pump, energized by a large solar reflector, was built by A.G.Eneas in 1901. In 1908, H. G. Willsie and John Boyle, Jr. built a 15kW solar engine, but the project was financial failure. Frank Shuman made solar powered engine using flat plate collector which was commercially successful. A solar still was built by J. Harding and C. Wilson for fresh water production in desert areas. In 1950, Chaplin, Fullen and Pearson

developed the first solar cell. In 1959. the first successful Vanguard satellite carried solar chips providing power for space applications.

2.2 Literature Survey

Though. we had different type of solar collectors by the end of the ninenteenth century. they were not used in day today life because of many problems associated with them. They were costly in comparison to conventional methods as well as their use was quite troublesome.

The main problem with the solar energy utilization is its low intensity and uncertainty regarding availability. Many people have worked in the field of energy storage devices to overcome the difficulty of the uncertainty. Due to low intensity of the solar energy. heat collection efficiency decreases rapidly with the outlet temperature. Use of multiple covers to reduce the front heat losses has been analyzed by many researchers. Use of concentrating reflectors is a costly affair. but is important in the case of higher temperature requirements. According to Collares Pereira and Sequeira, 1982 . Compound Parabolic Concentrator reflector with low concentration and non-evacuated receivers may be economical for temperatures around 100 °C [14]. O'Gallagher et al 1982, achieved efficiency of about 50% around 200 °C with fixed tilt evacuated collector using glass tubes shaped as compound parabolic concentrator [14]. The next possible step was to get the optimum orientation of the collector. so that maximum energy can be harnessed. Many researchers have done work in this direction. [33] The next step was to reduce the heat losses from the cover. People tried to use the selective coating on the absorber surface so that it absorbs maximum of the solar radiation

falling on it but emits the least thermal radiation back to the cover. It was found difficult to use these selective coatings in everyday life because selective coatings need very careful operation to protect them from damage. The other way to reduce loss is to reduce the convective loss inside the cover gaps, which will result in increased collection efficiency because of the increased resistance to the heat flow towards the atmosphere through the cover. For this purpose people are trying to evacuate the gap between the two cover sheets [28],[32]. Glass is the most popular cover material used because of its transmission properties, but it can not withstand any compression as it is very brittle. Thus evacuating the cover gap is not an easy task. The natural configuration for this is the tube form. All of the evacuated collectors must use a selective absorber coating to reduce the radiative losses at high temperatures. People are using different arrangements to make it possible but no one has got very satisfactory results. The third way to reduce the losses may be the use of the radiation absorbing media either fluid or the liquid. The present work is to check feasibility of the use of the gaseous media for the purpose of increasing the heat collection efficiency along with the temperature. The use of this property of the radiation absorbing gaseous media has been studied in a different way and also in a different application 'In solar thruster' by Venkateswaran et al [5]. The emissivity of the gases like CO_2, NH_3 etc. has been theoretically and experimentally obtained by researchers like Hottel [8]. Methods have been evolved for calculating radiant heat exchange in a gas filled enclosure with gray walls and isothermal gas by Hottel and Mangelsdorf [6] and Eckert. Bevan and Dunkle [3] had given the method for calculating radiation exchange in an generalized case using the band measurement datas. Measurements by Howard, Burch and Wiliams [1] give the band absorption for the complete spectrum of the gas at room temperature. Hottel and

Cohen [7] have worked in the direction to get the allowance for nonuniformity of the gas temperature. Edward [1] also suggested the methodology to solve the case when enclosure is of nongray walls and gas is isothermal.

2.3 Present work

The present work is aimed at the study of the effect of the use of the radiation absorbing gaseous media in flat plate solar collectors. A computer program has been made for the purpose of the theoretical study. It is made for tracking collector in polar mode and for nontracking collector. The geometry of the collector is so designed to extract the maximum amount of the energy.(For details refer Chapter : Experimental set-up) Emissivity of the gaseous media have been taken from Hottel's Emissivity Charts. Program has been made for transient study of the collector. A model of the collector had been fabricated and tested for Ammonia. The analysis of the effect of evacuating the whole collector has also been studied and the gain in the temperature and the collection efficiency has been compared for different cases.

The results obtained show sufficient gain in temperature and collection efficiency at higher temperatures in the case of absorbing media. At large flow rates, there is negligible gain in the efficiency and outlet temperatures. The gain is increasing with the increase in the working fluid outlet temperature. The experimental results also showed increase in the efficiency when gas (NH_3) was used. Thus the computational results are verified qualitatively. Since the use of these absorbing media is neither a costly affair nor it causes any severe problems except leakage of the gas, it can be implemented easily in all types of the solar collectors where the leakage can be avoided.

Chapter 3

Fundamental Concepts

3.1   Solar Energy

3.1.1   The Sun and Solar Energy

The source of solar energy is the Sun, which is a gaseous star (approximately 80%
Hydrogen and 18% Helium).For all practical purposes. it may be considered to be ra-
diating energy at an effective temperature of 5760 °K. The spectrum of the wavelength
of radiation stretches from 0.29 to 4.75μm. The maximum radiation intensity is found
at wavelength of 0.50μm. In order to calculate the beam and diffuse solar radiation in-
tensities on different days and at different times of the day at different locations on the
earth, the solar geometry and the location of the place of interest need to be defined.
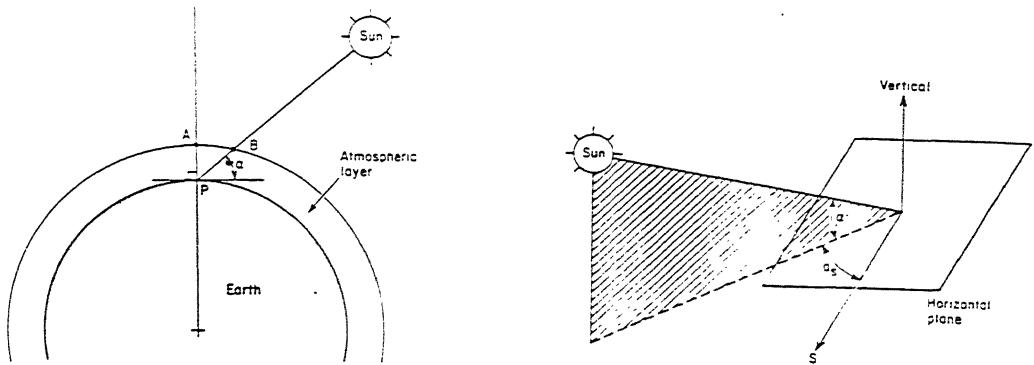
Figure 2: Solar Altitude and Azimuth angles with reference to local horizontal plane for North Hemisphere. [12]

3.1.2   Solar Geometry

It is adopted that the sun moves on an imaginary spherical surface called celestial sphere and this sphere is sufficiently large so that the sun can be considered as a point. The celestial sphere is assumed to be centered at the site of interest on the earth's surface. Since the sun is moving on a sphere, (i.e. two degrees of freedom), two angles are required to define the instantaneous position of the sun.

[1] Solar Altitude angle α

It is measured from the local horizontal plane upwards to the center of the sun. It is zero at sunrise and sunset and maximum at solar noon. (See Figure 2)

[2] Solar Azimuth angle a_s

It is measured from in the horizontal plane between the north-south line and the projection of the sun's rays onto the horizontal plane. It is zero at the local solar noon, positive before noon and negative after noon. (See Figure 2)

The solar altitude and azimuth angles are related to the solar hour angle the latitude L. and the solar declination δ_s. The solar altitude angle α. is given by

$$sin(\alpha) = sin(L)\ sin(\delta_s) + cos(L)\ cos(\delta_s)\ cos(H_s) \quad (sin(\alpha) >= 0) \tag{1}$$

The solar azimuth angle a_s is given by

$$sin(a_s) = \frac{cos(\delta_s)\ sin(H_s)}{cos(\alpha)} \tag{2}$$

Other angles which come into calculations are.

[1] Latitude L

It is the angle between the earth's equatorial plane and a line from the center of the earth to the site of interest. It is positive in the north of the equator and negative in the south.

[2] Hour angle H_s

It is given by 15 ° times the number of the hours from local solar noon. It is zero at noon. positive before noon and negative after noon. [The signs of the angles are based on the usual positive angular displacement rule in right hand coordinate systems.] The expression for Hour angle is.

$$H_s = 12.0 - corrected\ standard\ time - ET/60 \tag{3}$$

Where ET is the Equation of time, which is the difference between standard clock time and the solar time. (This happens because the length of the solar day varies due to the tilt of the earth's axis. the nonspherical shape of the earth and the orbital eccentricity.

) It is expressed in minutes and its values are tabulated in Appendix A,Table 7
An empirical equation for calculating the ET values is given by Duffie and Beckman
1980 [14].

$$ET = 9.87 \, sin(2B) \; - \; 7.53 \, cos(B) \; - \; 1.5 \, sin(B) \tag{4}$$

Where B is $\frac{2\pi(N_{day} - 81)}{364}$ for N_{day}, and N_{day} is the number of the day i.e. 1 for January,
1 and 365 for december, 31.
The corrected standard time for west of Greenwich, is defined as.

$$
\begin{aligned}
Corrected \; standard \; time \quad &= \quad Standard \; clock \; time \\
&+ \quad (time \; zone \; meridian \; - \; local \; site \; longitude \,)/15
\end{aligned}
$$

[3] Solar Declination δ_s

It is the angle formed by the line from center of the earth to the center of the sun
at noon on a particular day and the plane containing the earth's equator.(See Figure
3) Cooper suggests the approximate equation

$$\delta_s = 23.45 \, sin \left(\frac{2\pi(284 + N_{day})}{365} \right) \tag{5}$$

For engineering purposes, the declination is assumed to be constant over a day. The
declination is considered positive when sun is in the northern latitudes and negative
when in the southern latitudes. On June 21, summer solstice, sun is at its northern
extreme position hence declination is maximum positive and is the longest day in
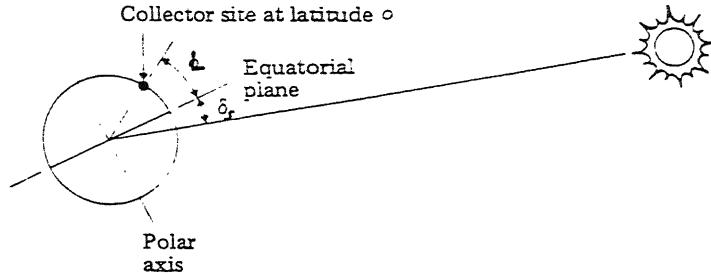
Figure 3: Solar Declination angle

northern hemisphere. On December 21. winter solistice. sun is at its southern extreme.
hence declination is maximum negative and is the shortest day in northern hemisphere.

3.1.3   Solar Incidence angle θ_i

The solar incidence angle is the angle between the normal to the irradiated surface and
a line collinear with the sun's rays. The solar incidence angle for any fixed surface is
given by

$$
\begin{aligned}
cos(\theta_i) \quad = \quad & sin(\delta_s)[sin(L)\ cos(\beta) - cos(L)\ sin(\beta)\ cos(a_c)] \\
& +cos(\delta_s)\ cos(H_s)\ [cos(L)\ cos(\beta) + sin(L)\ sin(\beta)\ cos(a_c)] \\
& +cos(\delta_s)\ sin(\beta)\ sin(a_c)\ sin(H_s)
\end{aligned}
\tag{6}
$$

where β is the surface tilt angle from local horizontal and a_c is the surface azimuth
angle defined analogously to the solar azimuth angle a_s.

The angle β is positive for a south facing surfaces and negative for north facing
surfaces. The negative value of $cos(\theta_i)$ indicates that $\theta_i > 90$ ° and the sun's rays do
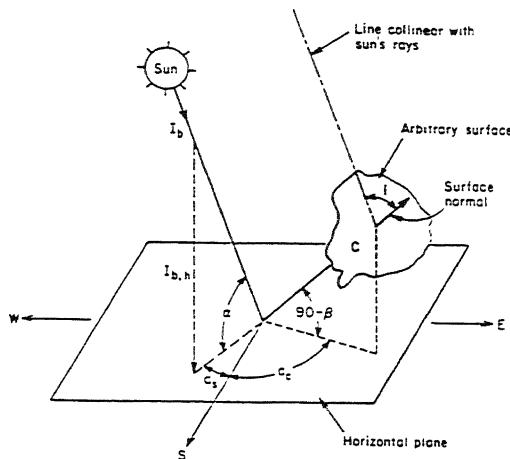
Figure 4: Angles for Determination of Incidence angle [12]

not strike the surface.

3.1.4 Incidence angles for Tracking Collectors

Tracking is required. mainly in the case of concentrating type of collectors, to maintain the sun within their field of view and to minimize the incidence angle. Either one or two degree of freedom modes can be used according to the requirements.

For perfect tracking, $cos(\theta_i)$=1.0 Single axis tracking can involve either a horizontal. east-west axis or a horizontal. north-south axis of rotation. Also a polar mount can be used which employs a north-south axis tilted up at an angle equal to the local latitude.

The incidence angle for these modes is,

1 East-West axis Horizontal

$$cos(\theta_i) = (1 - cos^2(\alpha)\ sin^2(a_s))^{1/2} \tag{7}$$

2 North-South axis Horizontal

$$cos(\theta_i) = (1 - cos^2(\alpha)\ sin^2(a_s))^{1/2} \tag{8}$$

3 Polar axis

$$cos(\theta_i) = cos(\delta_s) \tag{9}$$

3.1.5 The Extraterrestrial Solar Radiation

The mean annual value of the radiation intensity normal to sun's rays incident upon a plane surface situated in the outer limits of the earth's atmosphere is called the solar constant. It varies inversely with the square of the distance from the center of the sun. The earth axis of rotation is tilted 23.5 ° with respect to its orbit around the sun, therefore, solar constant varies with location (latitude). The present accepted standard values of the solar constant [determined by Thekackara and Drummond] is 1353 W/m^2. The spectral distribution of the extraterrestrial radiation, Figure 5 is

Ultra-violet region range 0.00 to 0.38μm 7.0%

Visible region   range 0.38 to 0.78μm 47.3%

Infra-red region   range 0.78 to $\infty\mu$m 45.7%

The value of the extraterrestrial solar radiation changes with the position of the sun because of the elliptic orbit of the sun. (Appendix A,Table 8   ) The equation for the value of the extraterrestrial solar radiation is

$$I_o = I_{sc}\left[1.0\ +\ 0.034\ cos\left(\frac{2\pi N_{day}}{365}\right)\right] \tag{10}$$

The value of the extraterrestrial horizontal solar intensity at any time is given by
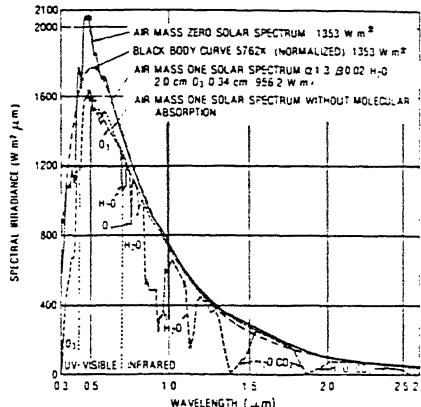
Figure 5: The Extraterrestrial Solar Spectrum and Molecular Absorption Bands of Gases in Atmosphere

$$I_{oh} = I_o \left[sin(\delta_s) \, sin(L) + cos(\delta_s) \, cos(L) \, cos(H_s) \right] \tag{11}$$

3.1.6   The Terrestrial Solar Radition

As the solar energy filters through the earth's atmosphere, it heats the atmosphere by molecular absorption and a part of it is scattered in new directions by molecules, water droplets, ice crystals, dust particles etc. Loss of energy through scattering and molecular absorption occurs mainly in visible range, whereas, loss in the infrared range is caused by absorption by water vapor and CO_2 present in the atmosphere (Figure 5).

This results in a net loss of 0 to 80% of the extra-terrestrial solar heat flux. The remaining, 0 to 80%, arriving at earth's surface, now, consists of two components, first is direct or beam radiation and the second is diffuse radiation. The direct or beam component appears to come directly from the sun and diffuse component is basically

from scattered and re-emitted energy by molecules in the atmosphere. The amount of the energy incident upon a terrestrial surface. pointed directly to the sun and its distribution in direct and diffuse components. depends upon atmospheric conditions. The terrestrial beam solar radiation intensity is given by.

$$I_b = I_o \left[a(K_T) \; K_T \; + \; b(K_T) \right] \tag{12}$$

Where K_T is the *Clearness index* or *atmospheric transmittance* and $a(K_T)$ and $b(K_T)$ are empirical coefficients (Appendix A.Table 9   ).

The Terrestrial horizontal solar intensity at any time is given by.

$$I_h = I_{oh} \; K_T \tag{13}$$

The Terrestrial horizontal diffuse solar intensity at any time is given by,

$$I_{dh} = I_h \; - \; I_b \; cos(\beta) \tag{14}$$

The diffuse solar radiation intensity on collector surface at any time is given by,

$$I_{dc} = I_{dh} \; cos^2(\frac{\beta}{2}) \tag{15}$$

3.1.7   Sky Radiation

Infrared radiation exchanges occurs between solar collector and the sky. Since the temperature of the deep space is about 2.7K, the effective sky temperature for radiation is usually below that of the ambient air temperature T_a. The net exchange $Q_{surface-sky}$

between a surface (gray) on the earth at temperature T_s . and emittance ϵ_s and the sky at effective temperature T_{sky} can be written as

$$Q_{surface-sky} = \epsilon_s \sigma (T_s^4 - T_{sky}^4) \qquad (16)$$

The sky radiation depends on the radiative properties of the sky (e.g. humidity and cloud cover) and many other secondary phenomena. An equation for $Q_{surface-sky}$ including principal climatic effects is given by deJong.

$$Q_{surface-sky} = \epsilon_s \sigma T_a^4 (0.39 - 0.009e)[1 - a_3(CC)] \qquad (17)$$
$$+ 4\epsilon_s \sigma T_a^4 (T_s - T_a)$$

Where e is the vapor pressure of atmospheric water vapor in mm Hg and CC is the cloud cover expressed in tenths . It is 1.0 for full overcast day and 0.0 for cloudless day. a_3 is the empirical constant (Appendix A.Table 10).

Thus the infrared radiation coming from the sky is,

$$Q_{sky} = \left[\frac{Q_{T_1}^u - Q_{surface-sky}}{(\tau_g^{in} + \alpha_g^{in})} \right] \qquad (18)$$

3.2 Transmissivity, absorptivity and reflectivity of glass sheet

The transmissivity τ_g, absorptivity α_g and reflectivity ρ_g of a glass sheet depends upon the refractive index n, absorption coefficient γ (the optical properties of glass) and the sheet thickness Δg.
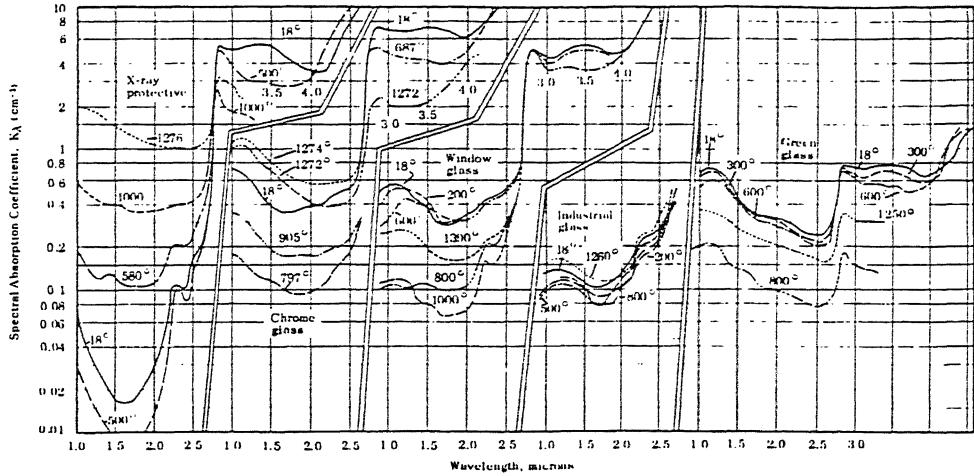
Figure 6: Spectral Absorption Coefficient for Different Types of Glasses [8]

3.2.1   Absorption coefficient γ

For microscopically homogeneous transparent media, Beer's law states that

$$I_\lambda(x) = I_\lambda(0)e^{-[\gamma_\lambda x/cos(\theta_i)]} \tag{19}$$

where x is the layer thickness and γ_λ is the absorption coefficient at wave-length λ.

Thus, for a single pass through the sheet, transmittance τ' and reflectance ρ' is

$$\tau' = e^{\frac{-\gamma \Delta q}{cos(\theta_i)}} \tag{20}$$

$$\rho'_\perp = \frac{sin^2(\theta_i - \theta_r)}{sin^2(\theta_i + \theta_r)} \quad \text{(for } \theta_i > 0.0)$$

$$\rho'_\parallel = \frac{tan^2(\theta_i - \theta_r)}{tan^2(\theta_i + \theta_r)} \quad \text{(for } \theta_i > 0.0)$$

$$= \frac{(n-1)^2}{(n+1)^2} \quad \text{(for } \theta_i = 0.0)$$
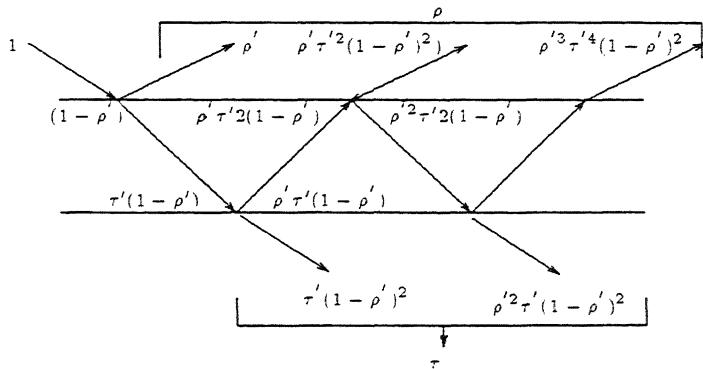
Figure 7: Ray Trace Diagram for Glass Sheet

In the case of sheet there is multiple reflections from the two interfaces, hence each of the. τ_g. α_g and ρ_g is expressed in the form of an infinite geometric series as a function of τ'. α' and ρ'. (See Figure 7) These equations are known as *Stoke's equation*. In the case of high absorption coefficient, the refractive index in the expression of reflectivity becomes complex number. i.e.

$$n_{eff} = n + \frac{\lambda k_\lambda}{4\pi} \tag{21}$$

It is very difficult to account this effect in exact manner, as the data for k_λ is not available. (See Figure 6) But some approximations are required for the reflection of the thermal radiation where absorption coefficient becomes very high. This effect can be incorporated by increasing the value of refractive index by some appropriate amount for calculation of reflection from the surface.

$$\tau_g = \tau' \left[1 + \frac{\tau'^2 (1 - \rho')^2}{1 - \rho'^2 \tau'^2} \right] \tag{22}$$

$$\rho_g \;=\; \rho' \left[\frac{(1 - \rho')^2}{1 - \rho'^2 \tau'^2} \right]$$

When both component of polarization are equal. the average reflectance and average transmittance are

$$\rho_g \;=\; 0.5[\rho(\rho'_\perp, \tau'_\perp) + \rho(\rho'_{||}, \tau'_{||})] \tag{23}$$

$$\tau_g \;=\; 0.5[\tau(\rho'_\perp, \tau'_\perp) + \tau(\rho'_{||}, \tau'_{||})]$$

$$\tag{24}$$

Once the values of effective transmittance and reflectance are calculated, the total absorptance can be calculated as

$$\alpha_g = 1 - \tau_g - \rho_g \tag{25}$$

3.3   The Emission of Radiation by Glass

In transparent materials. the emission and absorption of radiation is a bulk phenomena. Interaction of the simultaneous emission and absorption of radiation throughout the volume determines the rate at which radiation appears to be emitted by the surface. For a nonscattering dielectric material this rate depends upon the temperature, thickness of sheet, refractive index and absorption coefficient of the material.

3.3.1 Volume Emissive Power

According to McMahon [8], the spectral volume emissive power J_λ is a measure of the monochromatic power radiated at a given temperature by a unit volume of material into unit solid angle of space.

For isotropic materials, radiation is a diffuse process which proceeds uniformly in all directions.

$$j_\lambda = \frac{\gamma_\lambda n^2 W_{B\lambda}}{\pi} \qquad (26)$$

For a gray material, total volume emissive power is

$$j = \frac{\gamma n^2 W_B}{\pi} \qquad (27)$$

3.4 Geometric Mean Beam Length

In the case of absorbing and emitting media within an enclosure, the radiation from any differential surface element travels different path lengths to reach the other surface. The effect of these different path length can be expressed by a single mean path length known as Geometric Mean Beam Length. It is only dependent on geometry of the surfaces. Mathematically, It is defined as,

$$L_{kj}^m = \frac{1}{A_k F kj} \int_{A_j} \int_{A_k} \frac{cos(\beta_j) \, cos(\beta_k) \, dA_k \, dA_j}{\pi \, L^p} \qquad (28)$$

Where L^p is the path length and β is the angle made by L^p from the normal to the surface element dA.

The value of the geometric mean beam lengths for two parallel plates of side a and b separated by distance c and for two perpendicular plates of sides (a and b) and (b and c) have been calculated by Dunkle and Hottel [20]. The values calculated by Edward are given in Appendix B,Table 11 , 12

3.5   Gas Emissivity and Absorptivity

Until the early 1920s gas radiation was treated as a correction to the convective flux from a gas. The problem of evaluating the radiant heat transmission from gas flames received attention because of the practical importance in the design of the industrial furnaces and internal combustion engines.

A change in the occupancy of a particular energy level of the atom or molecules of a gas, can be viewed as emission or absorption of radiation in a narrow wavelength region. This process is known as line emission or absorption. This type of selective radiation spectrum is the characterstic of the gases. For monoatomic and diatomic gases, the capacity to emit and absorb radiation is insignificant, but in the case of poly-atomic gases like CO_2, water vapor, SO_2 and NH_3, they have considerable emissive power and high absorption capacity.

Gases with polar molecular form i.e. asymmetric molecules, exhibit energy transformations in the wavelengths of thermal radiation. The typical thermal energy transformation occurs as a result of changes in the vibrational frequency and rotation. This is manifested in a strong peak of energy emitted at a wavelength corresponding to the vibrational transformation, with multiple rotational energy emissions at wavelengths slightly different than the wavelength for vibrational energy. For this reason energy

emitted is usually described as a band of energy over a group of wavelengths from a rotational-vibrational transformation.

The result of this type of energy interaction is that gaseous absorption or emission occurs in discrete bands, giving a highly nongray behavior to the gases.

3.5.1 Gas Emissivity

The term gas emissivity has a meaning only in reference to emission from an isothermal gas shape to a specified portion of its bounding surface. It is the ratio of the incidence, on that surface portion, from gas lying within a specified field of view to the incidence from a black emitter at the gas temperature over the same field of view; and it is plainly dependent on the shape of the gas mass. The standard emissivity of a gas is that corresponds to a fixed path length.

Similarly, the standard gas absorptivity is the fractional absorption, by an isothermal gas, of blackbody radiation emitted from a bounding surface element through a fixed path length.

Similar to Kirchhoff's law for surfaces,

$$\epsilon_\lambda^{mix} = \alpha_\lambda^{mix} = 1 - e^{-(\gamma p L^m)} \tag{29}$$

The total emissivity and absorptivity are,

$$
\begin{aligned}
\epsilon^{mix} &= \frac{\int_0^\infty \epsilon_\lambda W_{\lambda,g} d\lambda}{\int_0^\infty W_{\lambda,g} d\lambda} \\
&= \frac{1}{\sigma T_g^4} \int_0^\infty \epsilon_\lambda W_{\lambda,g} d\lambda
\end{aligned}
\tag{30}
$$

$$\alpha_{mix} = \frac{\int_0^\infty \alpha_\lambda W_{\lambda,s} d\lambda}{\int_0^\infty W_{\lambda,g} d\lambda}$$

$$= \frac{1}{\sigma T_s^4} \int_0^\infty \alpha_\lambda W_{\lambda,s} d\lambda$$

(31)

Where T_s and T_g are the surface and the gas temperatures respectively.

3.5.2 Interrelation between Absorptivity and Emissivity

In terms of band black widths, the definitions of gas emissivity and gas absorptivity are

$$\epsilon^{mix}(T_g) = \frac{1}{\sigma T_g^4} \sum_i W_{\omega_i,g} A_{B_i}(T_g, pL^m)$$

(32)

$$\alpha^{mix}(T_g, T_s) = \frac{1}{\sigma T_s^4} \sum_i W_{\omega_i,s} A_{B_i}(T_s, pL^m)$$

(33)

(34)

Where A_{B_i} is the equivalant black width of a band.

Similarity between the above two equations, suggests the possibility of expressing absorptivities in terms of emissivities. If the emissivity is evaluated at the temperature of the surface, the right hand side of the Equation 33 and Equation 34 becomes identical with the exception that A_{B_i} is evaluated at T_s in the former and at T_g in the latter. Assumption of a constant absorption coefficient within a band gives

$$A_{B_i} = \Delta\omega(1 - e^{\alpha pL^m/\Delta\omega})$$

(35)

Using the temperature dependence of $\Delta\omega$ and α

$$\alpha(T_g, T_s, pL^m) = \left(\frac{T_g}{T_s}\right)^{0.5} \epsilon_g \left[T_s, pL^m \left(\frac{T_s}{T_g}\right)^{1.5}\right] \tag{36}$$

3.5.3 Gas Emissivity Charts

In view of the complexity of the theory and the associated uncertainty in the calculated values of gas emissivities, total radiation measurements are assumed to be most reliable and convenient source of information.

In spite of the highly nongray behavior of the gases, gray gas approximations are applicable in the case of energy exchange in systems where the walls are either black or nearly black.

The variables required to define total gas emissivity and absorptivity are

$$\epsilon^{mix} = f_1(L^m, p, P, C, T_g) \tag{37}$$

$$\alpha^{mix} = f_2(L^m, p, P, C, T_g, T_s) \tag{38}$$

Where C is the composition of the remainder gas. In most cases effect of C is negligible. If there is more than one emitting species in a gas, a correction factor is required to account for the overlap among the emission bands of the different molecules.

3.5.4 Emissivity Chart for CO_2

Radiation from CO_2 principally comes from bands at about 2.64 to 2.84, 4.13 to 4.50 and 13.0 to 17.0 microns. Rubens and Landenburg 1905 , Hottel and Mangelsdorf
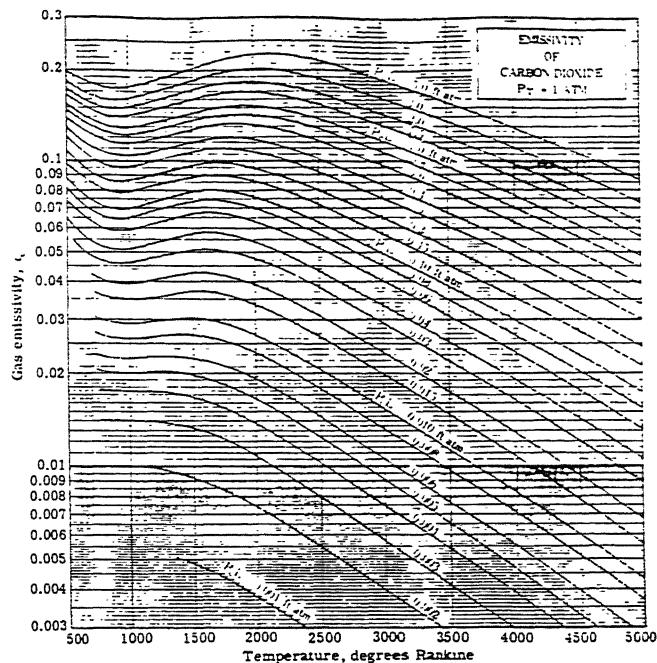
Figure 8: Emissivity Chart for CO_2 at 1 atmospheric total pressure [8].

1935 , Hottel and Smith 1935 and Eckert 1937 made total radiation measurements for CO_2 either in pure form or in mixture form. Emissivity chart for CO_2 prepared by Hottel is shown in Figure 8 .

The absorptivity and emissivity are correlated by

$$\alpha^{mix}(T_g, T_s, pL^m) = \left(\frac{T_g}{T_s}\right)^{0.65} \epsilon^{mix}\left(T_s, pL^m \frac{T_s}{T_g}\right) \tag{39}$$

3.5.5 Emissivity Chart for NH_3

Total radiation from ammonia vapor-nitrogen mixture has been measured by Port. The results are presented in the form of chart. The emissivity chart for NH_3 prepared by Port is shown in Figure 9 .

The absorptivity and emissivity are correlated by
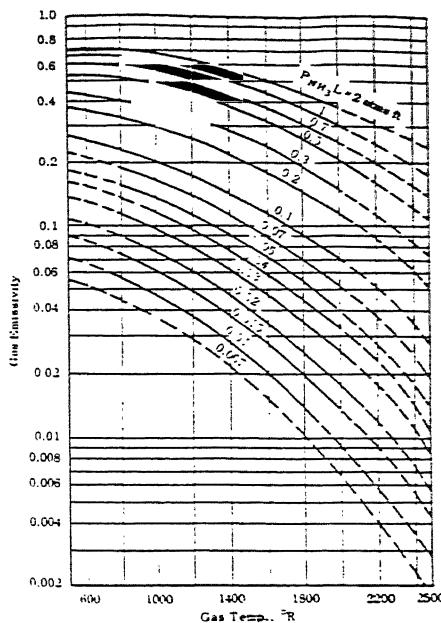
Figure 9: Emissivity Chart for NH_3 at 1 atmospheric total pressure [8].

$$\alpha^{mix}(T_g.T_s, pL^m) = \left(\frac{T_g}{T_s}\right)^{0.50} \epsilon^{mix}\left(T_s. pL^m \frac{T_s}{T_g}\right) \qquad (40)$$

3.5.6 Equation of Energy Transfer in Nongray Isothermal Gas

For analysis of the energy exchange in an enclosure that contains a nongray gas. the frequency band of interest is divided into absorption regions and window regions. In window regions, the gas is totally transparent. This causes two different types of expressions for energy transfer: one for regions of absorptance and other for the window regions (See Figure 10).

If the enclosure consists of n surfaces, each of which is assumed to have uniform radiosity, the equation of energy transfer for each wall for i^{th} absorption region is,
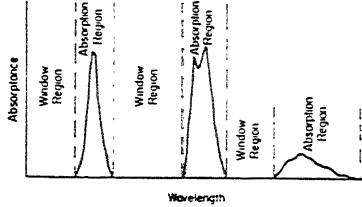
Figure 10: Band Division for Energy Exchange Calculations

$$G_{\nu,j}A_j = \sum_{k=1}^{n} J_{\nu,k}F_{kj}A_k\tau_{\nu_1} + \sum_{k=1}^{n} W_{b\nu_1}(T_g)F_{kj}A_k\alpha_{\Delta\nu_1} \qquad (41)$$

for $j = 1,2,3,....n$

for l^{th} window region is,

$$G_{\nu_l j}A_j = \sum_{k=1}^{n} J_{\nu_l k}F_{kj}A_k\tau_{\nu_1} \qquad (42)$$

for $j = 1,2,3,....n$

Where J_j is the radiosity of the jth surface, defined as

$$J_j = \rho_j G_j + W_j \qquad (43)$$

These sets of equations must be solved for all absorption and window regions and then results are summed up. Thus it is a very exhaustive technique, but unfortunately this is the only technique when walls are reflective. When the gray gas assumption are valid, the above equations are used with all quantities as total quantities.

$$G_j A_j = \sum_{k=1}^{n} J_k F_{kj}A_k\tau + \sum_{k=1}^{n} W_b(T_g)F_{kj}A_k\alpha \qquad (44)$$

Chapter 4

Mathematical Modelling

4.1   Assumptions

[1] Walls are gray and their emissivity and absorptivity are near to unity.

[2] Gas volume is isothermal.

These assumptions justify the use of Hottel's Emissivity charts.

[3] Pressure of the gas inside the gaps and box remains constant.

[4] No scattering takes place either by gas or glass volume. This makes the extinction coefficient equal to the absorption coefficient.

[5] Glass properties (absorption coefficient and refractive index) are wavelength independent, since the wavelengths are grouped in three regions, namely thermal, infra-red and solar.

[6] Beam solar radiation becomes diffuse when reflected by glass surface or walls.

[7] Since absorber plate is made of copper sheet, it's temperature is

uniform throughout the plate.

[8] The heat transfer to the working fluid takes place only from the one side of the channel. which is formed by the absorber plate itself.

[9] Reflectivity of the ground is negligible.

4.2   Notation for walls

The walls are numbered as,

1   : For upper cover

2,3 : For walls never facing sun's rays. i.e. walls in the direction perpendicular to surface azimuth line in the case of tracking collector and facing south in the case of nontracking collectors.

4   : For wall getting solar radiation after solar noon. also denoted by l.

5   : For wall getting solar radiation before solar noon. also denoted by r.

6   : For lower plate. also denoted by b.

Covers are numbered as 1 for top-most and N_{cover} for lower most.

Strips are numbered as 1 for lower most and N_x for upper most.

4.3   Solar Irradiation on Different Walls

Solar radiation falling on the collector cover consists of three components. namely beam or direct, diffuse and radiation reflected from ground. Intensity of beam solar radiation I_b is given by Equation 12 . The intensity of the diffuse solar radiation I_{dc} is given by Equation 15 . The total amount of diffuse solar radiation on collector cover is.

$$Q_{in}^{sd} = I_{dc} \, A_b \tag{45}$$

4.3.1 Direct Solar Radiation on Different Walls

Distribution of direct solar radiation on different walls depends on the angle of incidence (θ_h measured from the horizontal plane) of the rays. The distribution have been calculated for $\theta_h = 0$ to $\frac{\pi}{2}$ as it remains same for $\theta_h = \frac{\pi}{2}$ to π, except that the left and right wall irradiations are interchanged.

If $\left[\theta_h < \frac{\pi}{2}\right]$ then direct solar irradiation on left walls is always zero.

For $ig = 1, 2, \ \dots \ , N_{cover} - 1$ $\qquad Q_{in_{ig,l}}^{sb} = 0.0$

If $\left[\theta_h \leq tan^{-1}\left(\frac{\Delta_{gap} + \Delta_g}{L_a}\right)\right]$ then

$$Q_{in_{1,b}}^{sb} = I_b \, \tau_{e,1}^{sb} \, sin(\theta_h) A_b \tag{46}$$

$$Q_{in_{1,r}}^{sb} = I_b \, \tau_{e,2}^{sb} \, sin(\theta_h) A_b$$

$$Q_{in_{J,r}}^{sb} = 0.0$$

$$Q_{in_{J,b}}^{sb} = 0.0$$

for $j = 2, 3, \quad , (N_{cover} - 1)$

$$Q_{in_{B,r}}^{sb} = 0.0$$

$$Q_{in_{B,b}}^{sb} = 0.0$$

If $\left[tan^{-1}\left(\frac{ig\Delta_{gap} + \Delta_g}{L_a}\right) > \theta_h > tan^{-1}\left(\frac{(ig-1)\Delta_{gap} + \Delta_g}{L_a}\right)\right]$, for $ig = 2, 3, \quad \dots \quad , N_{cover}$

then

For $j = 1, 2. \quad .... \quad , (ig - 1)$,

$$Q^{sb}_{in_{j,b}} = I_b \, \tau^{sb}_{e,j} \, (sin(\theta_h)A_b - (j-1)(\Delta_{gap} + \delta_g)L_b cos(\theta_h)) \tag{47}$$

$$Q^{sb}_{in_{j,r}} = I_b \, \tau^{sb}_{e,j+1} \, \Delta_{gap}L_b cos(\theta_h)$$

For $j = ig$.

$$Q^{sb}_{in_{j,b}} = I_b \, \tau^{sb}_{e,j} \, (sin(\theta_h)A_b - (ig-1)(\Delta_{gap} + \Delta_g)L_b cos(\theta_h)) \tag{48}$$

$$Q^{sb}_{in_{j,r}} = I_b \, \tau^{sb}_{e,j+1} \, (sin(\theta_h)A_b - (ig-1)(\Delta_{gap} + \Delta_g)L_b cos(\theta_h))$$

For $j = (ig+1), (ig+2). \quad .... \quad , N_{cover} + 1$,

$$Q^{sb}_{in_{j,r}} = 0.0 \tag{49}$$

$$Q^{sb}_{in_{j,b}} = 0.0$$

$$Q^{sb}_{in_{B,r}} = 0.0 \tag{50}$$

$$Q^{sb}_{in_{B,b}} = 0.0$$

Where $\tau_{e,j}^{sb}$ is the effective transmissivity (without taking reflections into account but absorption by the gas in the covers is considered) of $(j-1)$ number of glass sheets placed in parallel. It is defined as,

$$\tau_{e,1}^{sb} = 1.0 \tag{51}$$

$$\tau_{e,2}^{sb} = \tau_g^{sb}$$

$$\tau_{e,3}^{sb} = \tau_g^{sb} \, \tau_{e,2}^{sb} \, \tau_{1,16}^{mix^{so}}$$

for $j = 3, 4, \quad .... \quad ..N_{cover} + 1$

$$\tau_{e,j}^{sb} = \tau_g^{sb} \, \tau_{e,(j-1)}^{sb} \, \tau_{j-2,16}^{mix^{so}}$$

If $\left[tan^{-1} \left(\left(\frac{N_{cover}\Delta_{gap} + (N_{cover}-1)\Delta_g + L_r)}{L_a} \right) \geq \theta_h > tan^{-1} \left(\frac{(N_{cover}-1)(\Delta_{gap} + \Delta_g)}{L_a} \right) \right]$ then,

For $ig = 1, 2, \quad .... \quad .N_{cover}$,

$$Q_{in_{ig,b}}^{sb} = I_b \, \tau_{e,ig}^{sb} \, (sin(\theta_h)A_b - (ig-1)(\Delta_{gap} + \Delta_g)L_b cos(\theta_h)) \tag{52}$$

$$Q_{in_{ig,r}}^{sb} = I_b \, \tau_{e,ig+1}^{sb} \, \Delta_{gap} L_b cos(\theta_h)$$

$$Q_{in_{B,b}}^{sb} = 0.0 \tag{53}$$

$$Q_{in_{B,r}}^{sb} = I_b \, \tau_{e,N_{cover}+1}^{sb} \, (sin(\theta_h)A_b - (N_{cover}-1)(\Delta_{gap} + \Delta_g)L_b cos(\theta_h))$$

If $\left[\theta_h > tan^{-1}\left(\frac{(N_{cover}\Delta_{gap}+(N_{cover}-1)\Delta_g+L_c)}{L_a}\right)\right]$ then,

For $ig = 1, 2, \quad .... \quad . N_{cover}$.

$$Q^{sb}_{in_{ig,b}} = I_b \tau^{sb}_{e,ig} \left(sin(\theta_h)A_b - (ig-1)(\Delta_{gap} + \Delta_g)L_b cos(\theta_h)\right) \qquad (54)$$

$$Q^{sb}_{in_{ig,r}} = I_b \tau^{sb}_{e,ig+1} \Delta_{gap}L_b cos(\theta_h)$$

$$Q^{sb}_{in_{B,b}} = I_b \tau^{sb}_{e,N_{cover}+1} \left(sin(\theta_h)A_b - ((N_{cover}-1)\Delta_{gap} + N_{cover}\Delta_g + L_c)L_b cos(\theta_h)\right) \qquad (55)$$

$$Q^{sb}_{in_{B,r}} = I_b \tau^{sb}_{e,N_{cover}+1} L_b L_c cos(\theta_h)$$

4.3.2 Total Incident Solar Flux on Different Walls

The beam or direct solar radiation falls only on three sides of the box and gaps, but absorptivity being less than unity, causes the reflection of the radiation resulting in the solar irradiation on other walls also. Since even the direct solar radiation changes its characterstic to approximately diffuse, the reflected solar radiation have been assumed to be uniformly diffuse in all directions.

For the irradiation of the solar radiation on the walls of the box, equations are

$$G^{so}_{B,1} = \sum_{j=2}^{6}(1 - \alpha^{so}_{B,j})F_{j1} \tau^{mix^{so}}_{B,1j} G^{so}_{B,j} \qquad (56)$$

$$G^{so}_{B,2} = \sum_{j=3}^{6}(1 - \alpha^{so}_{B,j})F_{j2} \tau^{mix^{so}}_{B,2j} G^{so}_{B,j} + \rho^{so}_g)F_{12} \tau^{mix^{so}}_{B,21} G^{so}_{B,1} + G'^{so}_{B,T}F_{12} \tau^{mix^{so}}_{B,12}$$

$$G_{B.3}^{'so} = \sum_{j=2,j\neq3}^{6} (1 - \alpha_{B,j}^{so})F_{j3} \tau_{B,3j}^{mix^{so}} G_{N,j}^{so} + \rho_g^{so})F_{13} \tau_{B.31}^{mix^{so}} G_{B.1}^{so} + G_{B.T}^{'so}F_{13} \tau_{B.13}^{mix^{so}}$$

$$G_{B.4}^{'so} = \sum_{j=2,j\neq4}^{6} (1 - \alpha_{B,j}^{so})F_{j4} \tau_{B.4j}^{mix^{so}} G_{B.j}^{so} + \rho_g^{so})F_{14} \tau_{B.41}^{mix^{so}} G_{B.1}^{so} + G_{B.T}^{'so}F_{14} \tau_{B.14}^{mix^{so}} + Q_{in_{B.i}}^{sb}$$

$$G_{B.5}^{'so} = \sum_{j=2,j\neq5}^{6} (1 - \alpha_{B,j}^{so})F_{j5} \tau_{B.5j}^{mix^{so}} G_{B.j}^{so} + \rho_g^{so})F_{15} \tau_{B.51}^{mix^{so}} G_{B.1}^{so} + G_{B.T}^{'so}F_{15} \tau_{B.15}^{mix^{so}} + Q_{in_{B.r}}^{sb}$$

$$G_{B.6}^{'so} = \sum_{j=2}^{5} (1 - \alpha_{B,j}^{so})F_{j6} \tau_{B,6j}^{mix^{so}} G_{B,j}^{so} + \rho_g^{so})F_{16} \tau_{B.61}^{mix^{so}} G_{B.1}^{so} + G_{B.T}^{'so}F_{16} \tau_{B.16}^{mix^{so}} + Q_{in_{B.b}}^{sb}$$

Where $G_{B.T}^{'so}$ is the diffuse solar radiation coming to the box through the upper side of the glass sheet.

For single glass cover.

$$G_{B,T}^{'so} = Q_{in}^{sd}\tau_g^{sd} \tag{57}$$

For multiple glass cover.

$$G_{B,T}^{'so} = G_{N_{cover}-1.6}^{'so}\tau_g^{sd} \tag{58}$$

For the irradiation of the solar energy on the walls of the gap. equations are

$$G_{ig,1}^{so} = \sum_{j=2}^{6}(1 - \alpha_{ig,j}^{so})F_{ig.j1} \tau_{ig,1j}^{mix^{so}} G_{ig,j}^{so} + F_{ig,16} \tau_{ig,16}^{mix^{so}} (G_{ig,L}^{'so} + \rho_g Q_{in_{ig,b}}^{sb}) \tag{59}$$

$$G_{ig,2}^{so} = \sum_{j=3}^{6}(1 - \alpha_{ig,j}^{so})F_{ig.j2} \tau_{ig,2j}^{mix^{so}} G_{ig,j}^{so} + \rho_g^{so})F_{ig,12} \tau_{ig,21}^{mix^{so}} G_{ig,1}^{so}$$

$$+ \quad F_{ig,12} \tau_{ig,12}^{mix^{so}} (G_{ig,L}^{'so} + G_{ig,T}^{'so} + \rho_g Q_{in_{ig,b}}^{sb})$$

$$G_{ig,3}^{so} = \sum_{j=2,j\neq3}^{6} (1 - \alpha_{ig,j}^{so})F_{ig.j3} \tau_{ig,3j}^{mix^{so}} G_{ig,j}^{so} + \rho_g^{so})F_{ig,13} \tau_{ig,1j}^{mix^{so}} G_{ig,1}^{so}$$

$$+ \; F_{ig,12} \; \tau_{ig,13}^{mix^{so}} \; (G_{ig,L}^{'so} + G_{ig,T}^{'so} + \rho_g Q_{in_{ig,5}}^{sb})$$

$$G_{ig,4}^{so} = \sum_{j=2,j\neq4}^{6} (1 - \alpha_{ig,j}^{so}) F_{ig,j4} \; \tau_{ig,4j}^{mix^{so}} \; G_{ig,j}^{so} + \rho_g^{so}) F_{ig,14} \; \tau_{ig,41}^{mix^{so}} \; G_{ig,1}^{so}$$

$$+ \; \tau_{ig,14}^{mix^{so}} \; [F_{ig,14}(G_{ig,L}^{'so} + G_{ig,T}^{'so} + \rho_g Q_{in_{ig,5}}^{sb}) + Q_{in_{ig,l}}^{sb}]$$

$$G_{ig,5}^{so} = \sum_{j=2,j\neq5}^{6} (1 - \alpha_{ig,j}^{so}) F_{ig,j5} \; \tau_{ig,5j}^{mix^{so}} \; G_{ig,j}^{so} + \rho_g^{so}) F_{ig,j1} \; \tau_{ig,51}^{mix^{so}} \; G_{ig,1}^{so}$$

$$+ \; \tau_{ig,15}^{mix^{so}} \; [F_{ig,15}(G_{ig,L}^{'so} + G_{ig,T}^{'so} + \rho_g Q_{in_{ig,5}}^{sb}) + Q_{in_{ig,r}}^{sb}]$$

$$G_{ig,6}^{so} = \sum_{j=1}^{5} (1 - \alpha_{ig,j}^{so}) F_{ig,j6} \; \tau_{ig,6j}^{mix^{so}} \; G_{ig,j}^{so} + \rho_g^{so}) F_{ig,16} \; \tau_{ig,61}^{mix^{so}} \; G_{ig,1}^{so} + \tau_{ig,15}^{mix^{so}} \; F_{ig,15} G_{ig,T}^{'so}$$

Where $G_{ig,T}^{'so}$ and $G_{ig,L}^{'so}$ are the diffuse solar radiation coming to the ig^{th} gap through the upper and the lower glass sheets as a result of transmission of the solar irradiation on the lower and the upper sides of the respective glass sheets.

4.4 Thermal Irradiation on Different Walls

Every wall emits thermal radiation at all temperatures and simultaneously absorbs the thermal radiation. The extent of emission and absorption is determined by the properties known as emissivity and absorptivity. In an enclosure walls radiate, absorb and reflect the radiation. Thus the irradiation on any wall consists of multi reflected and direct radiation from other walls.

For the box, irradiation of thermal radiation on different walls can be calculated as

$$G_{B,1}^{th} = \sum_{j=2}^{6} (1 - \alpha_{B,j}^{th}) F_{B,j1} \; \tau_{B,j1}^{mix^{th}} \; G_{B,j}^{th} \tag{60}$$

$$+ \quad \epsilon_{B.j} A_b \sum_{j=2}^{6} F_{B.1j} \, \tau_{B.j1}^{mix^{th}} \, \sigma T_{B.j}^4$$

$$+ \quad T_B^{mix} \sum_{j=2}^{6} \epsilon_{B.1j}^{mix} \, F_{B.1j}$$

$$G_{B.2}^{th} \quad = \quad \sum_{j=3}^{6} (1 - \alpha_{B.j}^{th}) F_{B.j2} \, \tau_{B.j2}^{mix^{th}} \, G_{B.j}^{th}$$

$$+ \quad \epsilon_{B.j} A_{B.2} \sum_{j=3}^{6} F_{B.2j} \, \tau_{B.j2}^{mix^{th}} \, \sigma T_{B.j}^4$$

$$+ \quad F_{B.12} \, \tau_{B.12}^{mix^{th}} \, (\rho_g^{th} G_{B.1}^{th} + G_{B.T}^{'th} + Q_{r_{Ncover}}^l)$$

$$+ \quad T_B^{mix} \sum_{j=1,j\neq 2}^{6} \epsilon_{B.2j}^{mix} \, F_{B.2j}$$

$$G_{B.3}^{th} \quad = \quad \sum_{j=2,j\neq 3}^{6} (1 - \alpha_{B.j}^{th}) F_{B.j3} \, \tau_{B.j3}^{mix^{th}} \, G_{B.j}^{th}$$

$$+ \quad \epsilon_{B.j} A_{B.3} \sum_{j=2,j\neq 3}^{6} F_{B.3j} \, \tau_{B.j3}^{mix^{th}} \, \sigma T_{B.j}^4$$

$$+ \quad F_{B.13} \, \tau_{B.13}^{mix^{th}} \, (\rho_g^{th} G_{B.1}^{th} + G_{B.T}^{'th} + Q_{r_{Ncover}}^l)$$

$$+ \quad T_B^{mix} \sum_{j=1,j\neq 3}^{6} \epsilon_{B.3j}^{mix} \, F_{B.3j}$$

$$G_{B.4}^{th} \quad = \quad \sum_{j=2,j\neq 4}^{6} (1 - \alpha_{B.j}^{th}) F_{B.j4} \, \tau_{B.j4}^{mix^{th}} \, G_{B.j}^{th}$$

$$+ \quad \epsilon_{B.j} A_4 \sum_{j=2,j\neq 4}^{6} F_{B.4j} \, \tau_{B.j4}^{mix^{th}} \, \sigma T_{B.j}^4$$

$$+ \quad F_{B.14} \, \tau_{B.14}^{mix^{th}} \, (\rho_g^{th} G_{B.1}^{th} + G_{B.T}^{'th} + Q_{r_{Ncover}}^l)$$

$$+ \quad T_B^{mix} \sum_{j=1,j\neq 4}^{6} \epsilon_{B.4j}^{mix} \, F_{B.4j}$$

$$g_{B.5}^{th} \quad = \quad \sum_{j=2,j\neq 5}^{6} (1 - \alpha_{B.j}^{th}) F_{B.j5} \, \tau_{B.j5}^{mix^{th}} \, G_{B.j}^{th}$$

$$+ \quad \epsilon_{B.j} A_5 \sum_{j=2,j\neq 5}^{6} F_{B.5j} \, \tau_{B.j5}^{mix^{th}} \, \sigma T_{B.j}^4$$

$$
\begin{aligned}
&+\quad F_{B,15}\, \tau_{B,15}^{mix^{th}}\, (\rho_g^{th} G_{B,1}^{\prime th} + G_{B,T}^{\prime th} + Q_{r N_{cover}}^{l}) \\
&+\quad T_B^{mix} \sum_{j=1,j\neq 5}^{6} \epsilon_{B,5j}^{mix}\, F_{B,5j} \\
G_{B,6}^{th} &= \sum_{j=2}^{5}(1 - \alpha_{B,j}^{th}) F_{B,j6}\, \tau_{B,j6}^{mix^{th}}\, G_{B,j}^{th} \\
&+\quad \epsilon_{B,j} A_b \sum_{j=2}^{5} F_{B,6j}\, \tau_{B,j6}^{mix^{th}}\, \sigma T_{B,j}^{4} \\
&+\quad F_{B,16}\, \tau_{B,16}^{mix^{th}}\, (\rho_g^{th} G_{B,1}^{\prime th} + G_{B,T}^{\prime th} + Q_{r N_{cover}}^{l}) \\
&+\quad T_B^{mix} \sum_{j=1}^{5} \epsilon_{B,6j}^{mix}\, F_{B,6j}
\end{aligned}
$$

Where $G_{B,T}^{\prime th}$ is the diffuse thermal radiation coming to the box through the upper side of the glass sheet.

For single glass cover,

$$
G_{B,T}^{\prime th} = Q_{sky} \tau_g^{in} \tag{61}
$$

For multiple glass cover,

$$
G_{B,T}^{\prime th} = G_{N_{cover}-1,6}^{th} \tau_g^{in} \tag{62}
$$

For the ig^{th} gap, irradiation of thermal radiation on different walls and glass surfaces can be calculated as

$$
\begin{aligned}
G_{ig,1}^{th} &= \sum_{j=2}^{5}(1 - \alpha_{ig,j}^{th}) F_{ig,j1}\, \tau_{ig,j1}^{mix^{th}}\, G_{ig,j}^{th} \\
&+\quad \epsilon_{ig,j} A_b \sum_{j=2}^{5} F_{ig,1j}\, \tau_{ig,j1}^{mix^{th}}\, \sigma T_{ig,j}^{4}
\end{aligned} \tag{63}
$$

$$+ \quad F_{ig,61} \, \tau_{ig,61}^{mix^{th}} \, (\rho_g^{th} G_{ig,6}^{th} + G_{ig,L}^{'th} + Q_{r_{ig+1}}^u)$$

$$+ \quad T_{ig}^{mix} \sum_{j=2}^{6} \epsilon_{ig,1j}^{mix} \, F_{ig,1j}$$

$$G_{ig,2}^{th} \quad = \quad \sum_{j=3}^{5} (1 - \alpha_{ig,j}^{th}) F_{ig,j2} \, \tau_{ig,j2}^{mix^{th}} \, G_{ig,j}^{th}$$

$$+ \quad \epsilon_{ig,j} A_b \sum_{j=3}^{5} F_{ig,2j} \, \tau_{ig,j2}^{mix^{th}} \, \sigma T_{ig,j}^4$$

$$+ \quad F_{ig,12} \, \tau_{ig,12}^{mix^{th}} \, (\rho_g^{th} G_{ig,1}^{th} + G_{ig,T}^{'th} + Q_{r_{ig}}^l)$$

$$+ \quad F_{ig,62} \, \tau_{ig,62}^{mix^{th}} \, (\rho_g^{th} G_{ig,6}^{th} + G_{ig,L}^{'th} + Q_{r_{ig+1}}^u)$$

$$+ \quad T_{ig}^{mix} \sum_{j=1, j \neq 2}^{6} \epsilon_{ig,2j}^{mix} \, F_{ig,2j}$$

$$G_{ig,3}^{th} \quad = \quad \sum_{j=2, j \neq 3}^{5} (1 - \alpha_{ig,j}^{th}) F_{ig,j3} \, \tau_{ig,j3}^{mix^{th}} \, G_{ig,j}^{th}$$

$$+ \quad \epsilon_{ig,j} A_b \sum_{j=2, j \neq 3}^{5} F_{ig,3j} \, \tau_{ig,j3}^{mix^{th}} \, \sigma T_{ig,j}^4$$

$$+ \quad F_{ig,13} \, \tau_{ig,13}^{mix^{th}} \, (\rho_g^{th} G_{ig,1}^{th} + G_{ig,T}^{'th} + Q_{r_{ig}}^l)$$

$$+ \quad F_{ig,63} \, \tau_{ig,63}^{mix^{th}} \, (\rho_g^{th} G_{ig,6}^{th} + G_{ig,L}^{'th} + Q_{r_{ig+1}}^u)$$

$$+ \quad T_{ig}^{mix} \sum_{j=1, j \neq 3}^{6} \epsilon_{ig,3j}^{mix} \, F_{ig,3j}$$

$$G_{ig,4}^{th} \quad = \quad \sum_{j=2, j \neq 4}^{5} (1 - \alpha_{ig,j}^{th}) F_{ig,j4} \, \tau_{ig,j4}^{mix^{th}} \, G_{ig,j}^{th}$$

$$+ \quad \epsilon_{ig,j} A_b \sum_{j=2, j \neq 4}^{5} F_{ig,4j} \, \tau_{ig,j4}^{mix^{th}} \, \sigma T_{ig,j}^4$$

$$+ \quad F_{ig,14} \, \tau_{ig,14}^{mix^{th}} \, (\rho_g^{th} G_{ig,1}^{th} + G_{ig,T}^{'th} + Q_{r_{ig}}^l)$$

$$+ \quad F_{ig,64} \, \tau_{ig,64}^{mix^{th}} \, (\rho_g^{th} G_{ig,6}^{th} + G_{ig,L}^{'th} + Q_{r_{ig+1}}^u)$$

$$+ \quad T_{ig}^{mix} \sum_{j=1, j \neq 4}^{6} \epsilon_{ig,4j}^{mix} \, F_{ig,4j}$$

$$G_{ig,5}^{th} = \sum_{j=2}^{4}(1 - \alpha_{ig,j}^{th})F_{ig,j5}\,\tau_{ig,j5}^{mix^{th}}\,G_{ig,j}^{th}$$

$$+ \quad \epsilon_{ig,j}A_b\sum_{j=2}^{4}F_{ig,5j}\,\tau_{ig,j5}^{mix^{th}}\,\sigma T_{ig,j}^{4}$$

$$+ \quad F_{ig,15}\,\tau_{ig,15}^{mix^{th}}\,(\rho_g^{th}G_{ig,1}^{th} + G_{ig,T}'^{th} + Q_{r_{ig}}^{l})$$

$$+ \quad F_{ig,65}\,\tau_{ig,65}^{mix^{th}}\,(\rho_g^{th}G_{ig,6}^{th} + G_{ig,L}'^{th} + Q_{r_{ig+1}}^{u})$$

$$+ \quad T_{ig}^{mix}\sum_{j=1,j\neq 5}^{6}\epsilon_{ig,5j}^{mix}\,F_{ig,5j}$$

$$G_{ig,6}^{th} = \sum_{j=2}^{5}(1 - \alpha_{ig,j}^{th})F_{ig,j6}\,\tau_{ig,j6}^{mix^{th}}\,G_{ig,j}^{th}$$

$$+ \quad \epsilon_{ig,j}A_b\sum_{j=2}^{5}F_{ig,6j}\,\tau_{ig,j6}^{mix^{th}}\,\sigma T_{ig,j}^{4}$$

$$+ \quad F_{ig,16}\,\tau_{ig,16}^{mix^{th}}\,(\rho_g^{th}G_{ig,1}^{th} + G_{ig,T}'^{th} + Q_{r_{ig}}^{l})$$

$$+ \quad T_{ig}^{mix}\sum_{j=1}^{5}\epsilon_{ig,6j}^{mix}\,F_{ig,6j}$$

Where $G_{ig,T}'^{th}$ and $G_{ig,L}'^{th}$ are the diffuse thermal radiation coming to the ig^{th} gap through the upper and the lower glass sheets as a result of transmission of the solar irradiation on the lower and the upper sides of the respective glass sheets.

4.5 Heat Transfer to Fluid in Flow channels

Rectangular channels are attached to the absorber plates, hence heat is transferred from the absorber plate to heat extracting fluid by the side, which is formed by the absorber plate. The channels are made up of G.I. sheet, hence the heat transfer by remaining three walls of the channels can be neglected (as conductivity of G.I. sheet is not good to increase the temperature of these walls).

When the fluid flows inside the channel, it is heated up as it moves forward. Here analysis for one channel is given, which can be used for all channels by putting appropriate channel length l and fluid inlet temperature T_{f_i} . The absorber plate temperature of the face receiving solar radiation T_{p_o} is assumed to be uniform through out the plate and temperature of the inner side T_{p_i} is assumed to be uniform for each channel individually.

The energy balance for a differential element of length ∂x at a distance x from the inlet leads to the equation

$$h \ L_{ch} \partial x \left(T_{p_i} - T_{f(x)} \right) = \rho_f A_{ch} V_f C p_f \, \partial T_{f(x)} \tag{64}$$

or,

$$\frac{\partial T_{f(x)}}{(T_{p_i} - T_{f(x)})} = \left[\frac{\rho_f A_{ch} V_f C p_f}{h \ L_{ch}} \right]^{-1} \partial x$$

On Integration, this gives

$$T_{p_i} - T_{f(x)} = C_1 e^{-\left[\frac{\rho_f A_{ch} V_f C p_f}{h L_{ch}} \right]^{-1} x} \quad \text{If } T_{p_i} > T_{f(x)}$$

Applying the inlet condition results

$$T_{f_o} = T_{p_i} - (T_{p_i} - T_{f_i}) e^{-\left[\frac{\rho_f A_{ch} V_f C p_f}{h L_{ch}} \right]^{-1} l}$$

The value of the T_{p_i} can be calculated as,

$$\frac{K_p l L_{ch}}{\Delta_p} (T_{p_o} - T_{p_i}) = \rho_f A_{ch} V_f (T_{f_o} - T_{f_i}) C p_f \tag{65}$$

Rearrangement of the terms yields,

$$T_{p_i} = T_{p_o} - \left[\frac{\Delta_p \rho_f A_{ch} V_f C p_f}{l L_{ch} K_p} \right] (T_{f_o} - T_{f_i})$$

These equations are solved iteratively. until the values of T_{f_o} and T_{p_t} are within the desired accuracy for two consecutive iterations.

The convective heat transfer coefficient for the flow of fluid in the channel is obtained by using the correlation for forced flow in a circular pipe of equivalent diameter [12].

$$h = 0.0155 \, R_{e_D}^{0.83} \, Pr_f^{0.5} \, \frac{K_w}{D_{eq}} \qquad (66)$$

The values of the Prandtl number and Thermal conductivity of the fluid are calculated at mean fluid temperature. Total heat transferred to the fluid is obtained by summing up heat gains by all the channels.

For the case of high temperature working fluids, heat transfer coefficient are given in the form of.

$$h = 1.62 \left(\frac{V_f}{l \, D_{eq}} \right)^{\frac{1}{3}} f \qquad (67)$$

Where f is given for different temperatures in [30].   for the case of laminar flow inside tubes.

4.6   Convective Heat Loss From The Plates

For the ease of the analysis all the absorber plates and glass sheets are assumed at a uniform temperature at surface. Empirical correlations have been used for calculating the convective heat transfer coefficients.

4.6.1 Correlation for heat transfer coefficient from Glass surface to atmosphere

For Convective heat loss from the outer side of the glass cover to the environment. ASHRAE Fundamental Volume [23] recommends the correlation for average coefficient of heat transfer for all orientation of surface

$$h = 5.50 + 2.70\, V_{air} \tag{68}$$

4.6.2 Correlation for natural convection heat transfer coefficient from an inclined plate in rectangular enclosure

For heat loss from the heated plate inclined at an angle β from the horizontal, due to natural convection, the most recent and reliable correlation for comparative collector design studies, is given by Hollands [16],

$$
\begin{aligned}
Nu &= 1.0 + 1.44 \left[1 - \left(\frac{1708}{Gr\,Pr\,cos(\beta)} \right) \right]^{(+)} \left[1 - \frac{sin^{1.6}(1.8\beta)\,1708}{Gr\,Pr\,cos(\beta)} \right] \\
&+ \left[\left(\frac{Gr\,Pr\,cos(\beta)}{5830} \right)^{\frac{1}{3}} - 1 \right]^{(+)}
\end{aligned}
\tag{69}
$$

Where only positive values of the quantities in bracket with the (+) exponent are used and are taken as zero for negative values. The correlation is valid for the range of β from 0 to 75 ° of inclinations.

4.6.3 Correlation for natural convection heat transfer coefficient from vertical heated and cooled plates

The correlation given by Churchill and Chu [27] is.

$$Nu_L = 0.680 + 0.670\ Ra_L^{\frac{1}{4}}\left[1 + \left(\frac{0.492}{Pr}\right)^{\frac{9}{16}}\right]^{\frac{-4}{9}} \tag{70}$$

for $\quad 0 < Ra_L < 10^9$

$$= \left(0.825 + 0.387\ Ra_L^{\frac{1}{6}}\left[1 + \left(\frac{0.492}{Pr}\right)^{\frac{9}{16}}\right]^{\frac{-8}{27}}\right)^2$$

for $\quad 10^9 < Ra_L$

All properties except β in Gr are to be calculated at mean film temperature i.e. $\left(\frac{T_{surface} + T_{fluid}}{2}\right)$ and β to be calculated at T_{fluid}.

4.6.4 Correlation for natural convection heat transfer coefficient from inclined heated and cooled plates

Rich [21] recommended the use of $g\ cos(\theta)$ for plates inclined at an angle θ from vertical. His results are substantially correct for lower surface of a heated plate or the upper surface of the cooled plate. Thus convective heat transfer coefficient for wall 2 is obtained using this correlation. For the upper surface of a heated plate and the lower surface of the cooled plate. the boundary layer becomes unstable and separates at low Gr values. This has been studied experimentally by Fujii [25]. For this unstable case. he recommended the following correlations,

$$Nu_L = 0.13 \, Ra_L^{\frac{1}{3}} \quad \text{for } Ra_L > 5 \, 10^8 \tag{71}$$

$$Nu_L = 0.16 \, Ra_L^{\frac{1}{3}} \quad \text{for } Ra_L < 5 \, 10^8$$

Where Gr is based on $g \cos(\theta)$.

4.6.5 Correlation for natural convection heat transfer coefficient from vertical plate

Chapman [21] recommends the following correlation.

$$Nu_{L_c} = \frac{0.637 \, Ra^{0.25}}{1 + \frac{0.861}{Pr}} \tag{72}$$

Where L_c is the ratio of Area to Perimeter.

4.7 Modeling of Glass Sheet

When a solar or thermal flux passes through the glass sheet. it is absorbed in the sheet according to Beer's law. Thus absorption is not uniform throughout the thickness. Similarly. the emission from the glass sheet is also a bulk phenomena. which causes self- absorption of the emitted radiation. Thus the analysis of the glass sheet is done by dividing the thickness in N_x strips of equal thickness. Energy balance equation is written for all strips and then solved with the equations of the energy balance for other parts of the system.

4.7.1 Radiation Emitted By Glass Sheet and Strip-wise Absorption of Primary Radiation

The Beer's law has dependence on the direction of the radiation. because effective path length that the radiation travels is

$$\Delta L_e = \frac{\Delta x}{cos(\theta)} \tag{73}$$

To account this direction dependence. absorption and emission from each strip is calculated in different directions and then summed up using Simpson's rule to get the total absorption and emission.

If the end effects are neglected. emission from a strip of thickness ∂x per unit solid angle $\partial \omega$ is calculated using Equation 27 .

$$\partial E = \frac{\gamma_{th} n_{th}^2 W_B}{\pi} \partial \omega \partial x A_b \tag{74}$$

In the direction θ. the value of $\partial \omega$ is.

$$\partial \omega = sin(\theta) \partial \theta \partial \phi \tag{75}$$

Where θ varies from 0 to $\frac{\pi}{2}$ and ϕ from 0 to 2π.

Since emission is not dependent on angle ϕ, Equation 75 can be rewritten as,

$$\partial \omega = 2\pi sin(\theta) \partial \theta \tag{76}$$

Using this definition in Equation 74 .

$$\partial E = 2\gamma_{th} n_{th}^2 W_B sin(\theta) \, \partial \theta \, \partial x A_b \tag{77}$$

If the thickness ∂x is of the order of the inverse of the absorption coefficient. it is fairly correct to assume that no self absorption occurs inside the strip. Thus for a strip of finite thickness, the emission from each face can be calculated by doing integration over the strip thickness. Since the integral in θ direction can not be calculated analytically. Simpson's rule is here used to integrate in the θ direction.

Thus emission from each side of the ith strip of thickness Δx in direction θ is.

$$\Delta E_i(\theta) = 2\gamma_{th}\sigma n_{th}^2 A_b \Delta\theta \int_0^{\Delta x} T_g^4(x)sin(\theta)e^{-\left(\frac{\gamma_{th}x}{cos(\theta)}\right)} \partial x \tag{78}$$

Solving this. with the assumption that temperature inside the strip $T_g(x)$ remains same throughout the entire volume of the strip, we get

$$\Delta E_i(\theta) = 2\sigma n_{th}^2 A_b \Delta\theta\, T_g^4(x)tan(\theta)\left[1 - e^{-\left(\frac{\gamma_{th}\Delta x}{cos(\theta)}\right)}\right] \tag{79}$$

Now, numerical integration in the direction θ is done to calculate the total emission from the ith strip. Using Simpson's rule,

$$\Delta E_i = \frac{1}{3}\left[\Delta E_i(\theta = 0) + \Delta E_i(\theta = \frac{\pi}{2}) + 2\sum_{m=1}^{m=N_\theta/2}\left\{\Delta E_i((2m-1)\Delta\theta) + 2\Delta E_i(2m\Delta\theta)\right\}\right] \tag{80}$$

Now this emitted radiation from i^{th} strip is absorbed by the strips coming in its way to the surface. Thus the energy absorbed in the jth strip from the energy emitted by all other strips is.

$$\Delta Q_{abs_j}^P(\theta) = \sum_{i=1,i\neq j}^{N_x} \Delta E_i(\theta)e^{-\left(\frac{\gamma_{th}D_{i,j}}{cos(\theta)}\right)}\left[1 - e^{-\left(\frac{\gamma_{th}\Delta x}{cos(\theta)}\right)}\right] \tag{81}$$

Where $D_{i,j}$ is the center to centre distance between i^{th} and j^{th} strips less the thickness of one strip.

For getting total amount of the absorption i.e. $\Delta Q^p_{abs_j}$. Simpson's rule is applied in the same manner as applied to ΔE_i. This gives the absorption of the primary radiation emitted by various strips only. For getting the emission that goes from glass to outer medium, reflectivity calculations at the glass air or glass-gas interface are required. The emission those which are incident at angle more than the critical angle are completely reflected back and through multiple reflections, get absorbed in the bulk itself.

So firstly, the primary emission $Q^{u^p}_\tau$ and $Q^{l^p}_\tau$ from each strip reaching the interface is calculated and than the effect of interface reflectivity is accounted to get the total radiation emitted by the upper and lower surface of the glass sheet (Q^u_τ and Q^l_τ) and the absorption of the reflected primary radiation in each strip.

$$Q^{u^p}_\tau(\theta) = \sum_{i=1}^{N_x} \Delta E_i(\theta) e^{-\left(\frac{\gamma_{th} D_{i,u}}{\cos(\theta)}\right)} \tag{82}$$

$$Q^{l^p}_\tau(\theta) = \sum_{i=1}^{N_x} \Delta E_i(\theta) e^{-\left(\frac{\gamma_{th} D_{i,l}}{\cos(\theta)}\right)}$$

$$\tag{83}$$

Where $D_{i,u}$ is the distance between upper face of the ith strip and the upper surface of the sheet. Similarly, $D_{i,l}$ is the distance between lower face of ith strip and the lower surface of the sheet.

4.7.2 Strip-wise Self-absorption of Secondary radiation

Once the amount of the primary radiation reaching the interface in the direction θ, is known, multiple reflections of this is to be calculated. Transmissivity, reflectivity in

the direction θ is calculated using Equation 24. with a slight modification. that for angles greater than the critical angle reflectivity is unity.

$$\theta_{cr} = sin^{-1}\left(\frac{1}{n_{th}}\right) \tag{84}$$

If $\theta \geq \theta_{cr}$ then.

$$\tau_g'^{th} = 0.0 \tag{85}$$

$$\rho_{g\perp}'^{th} = 1.0$$

$$\rho_{g\|}'^{th} = 1.0$$

If $\theta < \theta_{cr}$ then.

$$\theta_r = sin^{-1}(n_{th} sin(\theta)) \tag{86}$$

$$\rho_{g\perp}'^{th} = \left(\frac{sin(\theta - \theta_r)}{sin(\theta + \theta_r)}\right)^2$$

$$\rho_{g\|}'^{th} = \left(\frac{tan(\theta - \theta_r)}{tan(\theta + \theta_r)}\right)^2$$

$$\tau_g'^{th} = e^{-\left\{\frac{\gamma_{th} L_g}{cos(\theta)}\right\}}$$

$$frac_{1\perp} = \frac{\rho_{g\perp}'^{th}\tau_g'^{th}(1 - \rho_{g\perp}'^{th})}{\left\{1 - \left(\rho_{g\perp}'^{th}\tau_g'^{th}\right)^2\right\}} \tag{87}$$

$$frac_{1\|} = \frac{\rho_{g\|}'^{th}\tau_g'^{th}(1 - \rho_{g\|}'^{th})}{\left\{1 - \left(\rho_{g\|}'^{th}\tau_g'^{th}\right)^2\right\}}$$

$$frac_{2_\perp} = \frac{(1 - \rho'^{th}_{g_\perp})}{\left\{1 - \left(\rho'^{th}_{g_\perp}\tau'^{th}_g\right)^2\right\}}$$

$$frac_{2_\parallel} = \frac{(1 - \rho'^{th}_{g_\parallel})}{\left\{1 - \left(\rho'^{th}_{g_\parallel}\tau'^{th}_g\right)^2\right\}}$$

$$frac_1 = 0.5(frac_{1_\perp} + frac_{1_\parallel})$$

$$frac_2 = 0.5(frac_{2_\perp} + frac_{2_\parallel})$$

$$Q^u_r(\theta) = frac_1\, Q^{lP}_r(\theta) + frac_2\, Q^{uP}_r(\theta) \tag{88}$$

$$Q^l_r(\theta) = frac_1\, Q^{uP}_r(\theta) + frac_2\, Q^{lP}_r(\theta)$$

In order to get total emission from each surface of the glass Simpson's rule is used to integrate in the θ direction from $\theta = 0$ to $\theta = \frac{\pi}{2}$.

$$Q^u_r = \frac{1}{3}\left[Q^u_r(\theta = 0) + Q^u_r(\theta = \frac{\pi}{2}) + 2\sum_{m=1}^{m=N_\theta/2}\left\{Q^u_r((2m-1)\Delta\theta) + 2Q^u_r(2m\Delta\theta)\right\}\right]$$

$$Q^l_r = \frac{1}{3}\left[Q^l_r(\theta = 0) + Q^l_r(\theta = \frac{\pi}{2}) + 2\sum_{m=1}^{m=N_\theta/2}\left\{Q^l_r((2m-1)\Delta\theta) + 2Q^l_r(2m\Delta\theta)\right\}\right]$$

For getting the energy absorbed in different strips due to secondary radiation i.e. multiply reflected part of the primary radiation from the interfaces, expression for energy absorbed in j^{th} strip is derived on the similar lines.

If $\theta \geq \theta_{sr}$ then,

$$\tau'_{g1} = 0.0 \tag{89}$$

$$\tau'_{g2} = 0.0$$

$$\tau_{g_{u,i}}^{'th} = e^{-\left(\frac{\gamma_{th} D_{i,u}}{\cos\theta_i}\right)}$$

$$\tau_{g_{l,i}}^{'th} = e^{-\left(\frac{\gamma_{th} D_{i,i}}{\cos\theta_i}\right)}$$

(90)

$$frac_{1_{\perp,j}} = \frac{\rho_{g\perp}^{'th}\left(\tau_{g_{u,i}}^{'th} + \rho_{g\perp}^{'th}\tau_g^{'th}\tau_{g_{l,i}}^{th}\right)}{\left\{1 - \left(\rho_{g\perp}^{'th}\tau_g^{'th}\right)^2\right\}}$$

(91)

$$frac_{1_{\|,j}} = \frac{\rho_{g\|}^{'th}\left(\tau_{g_{u,i}}^{'th} + \rho_{g\|}^{'th}\tau_g^{'th}\tau_{g_{l,i}}^{th}\right)}{\left\{1 - \left(\rho_{g\|}^{'th}\tau_g^{'th}\right)^2\right\}}$$

$$frac_{2_{\perp,j}} = \frac{\rho_{g\perp}^{'th}\left(\tau_{g_{l,i}}^{'th} + \rho_{g\perp}^{'th}\tau_g^{'th}\tau_{g_{u,i}}^{'th}\right)}{\left\{1 - \left(\rho_{g\perp}^{'th}\tau_g^{'th}\right)^2\right\}}$$

$$frac_{2_{\|,j}} = \frac{\rho_{g\|}^{'th}\left(\tau_{g_{l,i}}^{'th} + \rho_{g\|}^{'th}\tau_g^{'th}\tau_{g_{u,i}}^{'th}\right)}{\left\{1 - \left(\rho_{g\|}^{'th}\tau_g^{'th}\right)^2\right\}}$$

$$frac_{1_j} = 0.5(frac_{1_{\perp,j}} + frac_{2_{\|,j}})$$

$$frac_{2_j} = 0.5(frac_{2_{\perp,j}} + frac_{1_{\|,j}})$$

So, secondary energy absorbed in the jth strip is.

$$Q^s_{abs_j}(\theta) = frac_{1_j} Q_r^{up}(\theta) + frac_{2,j} Q_r^{lp}(\theta)$$

(92)

The above equation is integrated (using Simpson's rule) in the θ direction to get the total secondary absorption in j^{th} strip.

4.7.3 Strip-wise Absorption of Radiation Falling On Glass Sheet

When the radiation passes through the glass sheet. it is absorbed in different amounts at different locations depending on the length of path traveled by the radiation to reach the location and absorption coefficient γ.

$$\theta_r = \sin^{-1}\left(\frac{\sin(\theta)}{n_{so}}\right) \tag{93}$$

$$\rho_{g\perp}^{'sb} = \left(\frac{\sin(\theta - \theta_r)}{\sin(\theta + \theta_r)}\right)^2$$

$$\rho_{g\parallel}^{'sb} = \left(\frac{\tan(\theta - \theta_r)}{\tan(\theta + \theta_r)}\right)^2$$

$$\tau_g^{'sb} = e^{-\left\{\frac{\gamma_{so}L_g}{\cos(\theta)}\right\}}$$

$$\tau_{g_{u,i}}^{'sb} = e^{-\left(\frac{\gamma_{so}D_{i,u}}{\cos(\theta_r)}\right)} \tag{94}$$

$$\tau_{g_{l,i}}^{'sb} = e^{-\left(\frac{\gamma_{so}D_{i,l}}{\cos(\theta_r)}\right)}$$

$$Q_{d_{\perp,j}}^{'sb} = \frac{1 - \rho_{g\perp}^{'sb}\left(\tau_{g_{u,i}}^{'sb} + \rho_{g\perp}^{'sb}\tau_g^{'sb}\tau_{g_{l,i}}^{'sb}\right)}{\left\{1 - \left(\rho_{g\perp}^{'sb}\tau_g^{'sb}\right)^2\right\}} \tag{95}$$

$$Q_{d_{\parallel,j}}^{'sb} = \frac{1 - \rho_{g\parallel}^{'sb}\left(\tau_{g_{u,i}}^{'sb} + \rho_{g\parallel}^{'sb}\tau_g^{'sb}\tau_{g_{l,i}}^{'sb}\right)}{\left\{1 - \left(\rho_{g\parallel}^{'sb}\tau_g^{'sb}\right)^2\right\}}$$

$$Q_{d_j}^{'sb} = 0.5(Q_{d_{\perp,j}}^{'sb} + Q_{d_{\parallel,j}}^{'sb})$$

So. amount of beam solar radiation (in direction θ) absorbed in j^{th} strip $Q'^{sb}_{d_j}$ is.

$$Q^{sb}_{d_j} = \left(1 - e^{-\left[\frac{\gamma_{so}\Delta x}{\cos\theta_{rj}}\right]}\right) Q'^{sb}_{d_j} \qquad (96)$$

This gives the absorption of the radiation in the direction θ. In the case of diffuse solar radiation the above quantity is numerically integrated over $\theta = 0$ to $\frac{\pi}{2}$. Absorption of the thermal radiation is calculated using the same equations with γ_{th} instead of γ_{so} and n_{th} instead of n_{so}.

It gives the distribution of absorbed radiation falling on the outer side of the glass sheet. with 1st strip being the innermost and N_x the outermost.

$Q^{sb}_{d_j}$ distribution of beam solar radiation

$Q^{sd}_{d_j}$ distribution of diffuse solar radiation

$Q^{th}_{d_j}$ distribution of diffuse thermal radiation

$Q^{in}_{d_j}$ distribution of diffuse infrared radiation

4.7.4   Energy Balance Equations For Glass Covers

Once the absorption of the incident diffuse and beam solar radiation and thermal radiation in different strips. and emission of the thermal radiation from different strips and strip-wise self-absorption of the emitted thermal radiation are known. equations can be written to get the temperature increment of different strips after time Δt.

For outer glass cover

If there is only one glass covers. different radiations falling on the outer cover have been shown in Figure 11 .

For lowermost strip i.e. $j = 1$.
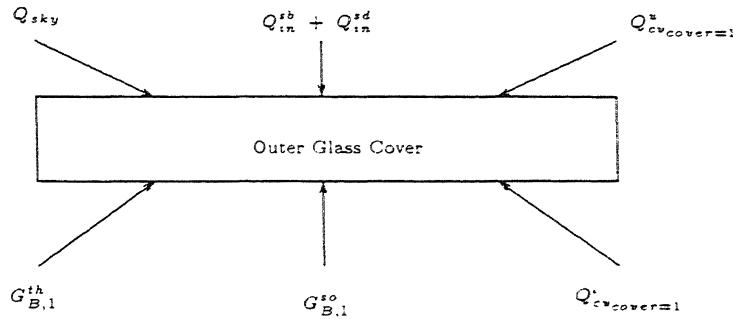
Figure 11: Incident Radiations on Outer Glass Sheet When Single Cover

$$
\begin{aligned}
\frac{\Delta T_{g,ig=1,j=1}}{\Delta t} =\ & [Q^p_{abs_{ig=1,j=1}} + Q^s_{abs_{ig=1,j=1}} - \Delta E_{ig=1,j=1} + Q_{sky}Q^{in}_{d_{j=1}} + Q^{sb}_{in_{1,b}}Q^{sb}_{d_{j=1}} \quad (97) \\
& + G^{th}_{B,1}Q^{th}_{d_{j=N_x}} + G^{so}_{B,1}Q^{so}_{d_{j=N_x}} - Q^l_{cv_{ig=1}} \\
& + \frac{K_g A_b}{D_x}(T_{g,ig=1,j=2} - T_{g,ig=1,j=1})]/(M_g Cp_g(\frac{1}{N_x}))
\end{aligned}
$$

For uppermost strip i.e. $j = N_x$,

$$
\begin{aligned}
\frac{\Delta T_{g,ig=1,j=N_x}}{\Delta t} =\ & [Q^p_{abs_{ig=1,j=N_x}} + Q^s_{abs_{ig=1,j=N_x}} - \Delta E_{ig=1,j=N_x} + Q_{sky}Q^{in}_{d_{j=N_x}} \quad (98) \\
& + Q^{sb}_{in_{1,b}}Q^{sb}_{d_{j=N_x}} + G^{th}_{B,1}Q^{th}_{d_{j=1}} + G^{so}_{B,1}Q^{so}_{i_{j=1}} - Q^u_{cv_{ig=1}} \\
& + \frac{K_g A_b}{D_x}(T_{g_{ig=1,j=N_x-1}} - T_{g_{ig=1,j=N_x}})]/(M_g Cp_g(\frac{1}{N_x}))
\end{aligned}
$$

For intermediate strips i.e. $j = 2$ to $j = N_x - 1$,

Figure 12: Incident Radiation on Outer Glass Sheet When Multiple Covers

$$\frac{\Delta T_{g,ig=1,j}}{\Delta t} = [Q^p_{abs_{ig=1,j}} + Q^s_{abs_{ig=1,j}} - \Delta E_{ig=1,j} + Q_{sky}Q^{in}_{d_j} + Q^{sb}_{in_{1,b}}Q^{sb}_{d_j} \quad (99)$$
$$+ \; G'^{th}_{B,1}Q^{th}_{d_{j=(N_x+1-j)}} + G'^{so}_{B,1}Q^{so}_{d_{j=(N_x+1-j)}}$$
$$+ \; \frac{K_g A_b}{D_x}(T_{g,ig=1,j+1} - 2T_{g,ig=1,j} + T_{g,ig=1,j-1})]/(M_g Cp_g(\frac{1}{N_x}))$$

If there is more than one glass covers. different radiations falling on the outer cover have been shown in Figure 12 .

For lowermost strip i.e. $j = 1$.

$$\frac{\Delta T_{g,ig=1,j=1}}{\Delta t} = [Q^p_{abs_{ig=1,j=1}} + Q^s_{abs_{ig=1,j=1}} - \Delta E_{ig=1,j=1} + Q_{sky}Q^{in}_{d_{j=1}} + Q^{sb}_{in_{1,b}}Q^{sb}_{d_{j=1}} (100)$$
$$+ \; G^{th}_{ig=1,1}Q^{th}_{d_{j=N_x}} + G'^{so}_{ig=1,1}Q^{so}_{d_{j=N_x}} - Q^l_{cv_{ig=1}}$$
$$+ \; \frac{K_g A_b}{D_x}(T_{g,ig=1,j=2} - T_{g,ig=1,j=1})]/(M_g Cp_g(\frac{1}{N_x}))$$

For uppermost strip i.e. $j = N_x$,

$$G^{th}_{Ncover-1,5} \qquad (Q^{th}_{in_{Ncover,b}} + G^{so}_{Ncover-1,5}) \qquad Q^{u}_{cv_{cover=Ncover}}$$

Inner Glass cover

$$G^{th}_{B,1} \qquad\qquad G^{so}_{B,1} \qquad\qquad Q^{i}_{cv_{cover=Ncover}}$$
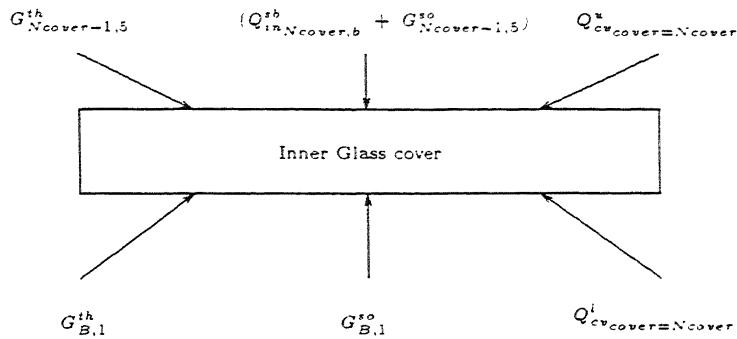
Figure 13: Incident Radiations on Inner Glass Sheet When Multiple Covers

$$
\frac{\Delta T_{g_{ig=1,j=N_x}}}{\Delta t} = [Q^p_{abs_{ig=1,j=N_x}} + Q^s_{abs_{ig=1,j=N_x}} - \Delta E_{ig=1,j=N_x} + Q_{sky}Q^{in}_{d_{j=N_x}} \quad (101)
$$

$$
+ \; Q^{sb}_{in_{1,b}}Q^{sb}_{d_{j=N_x}} + G^{th}_{ig=1,1}Q^{th}_{d_{j=1}} + G^{so}_{ig=1,1}Q^{so}_{d_{j=1}} - Q^u_{cv_{ig=1}}
$$

$$
+ \; \frac{K_g A_b}{D_x}(T_{g_{ig=1,j=N_x-1}} - T_{g_{ig=1,j=N_x}})]/(M_g C p_g(\frac{1}{N_x}))
$$

For intermediate strips i.e. $j = 2$ to $j = N_x - 1$.

$$
\frac{\Delta T_{g_{ig=1,j}}}{\Delta t} = [Q^p_{abs_{ig=1,j}} + Q^s_{abs_{ig=1,j}} - \Delta E_{ig=1,j} + Q_{sky}Q^d_{in_j} + Q^{sb}_{in_{1,b}}Q^{sb}_{d_j} \quad (102)
$$

$$
+ \; G^{th}_{ig=1,1}Q^{th}_{d_{j=(N_x+1-j)}} + G^{so}_{ig=1,1}Q^{so}_{d_{j=(N_x+1-j)}}
$$

$$
+ \; \frac{K_g A_b}{D_x}(T_{g_{ig=1,j+1}} - 2T_{g_{ig=1,j}} + T_{g_{ig=1,j-1}})]/(M_g C p_g(\frac{1}{N_x}))
$$

For inner glass cover

Different radiations falling on the inner cover have been shown in Figure 13 .

For lowermost strip i.e. $j = 1$.

$$\frac{\Delta T_{g_{ig=N_{cover},j=1}}}{\Delta t} = [Q^p_{abs_{ig=N_{cover},j=1}} + Q^s_{abs_{ig=N_{cover},j=1}} - \Delta E_{ig=N_{cover},j=1} \tag{103}$$

$$+ \quad Q^{sb}_{in_{ig=N_{cover},b}} Q^{sb}_{d_{j=1}} \tau^{mix^{so}}_{ig-1,16} + G^{th}_{ig=N_{cover}-1,5} Q^{th}_{d_{j=1}} + G^{so}_{ig=N_{cover}-1,5} Q^{so}_{d_{j=1}}$$

$$+ \quad G^{th}_{ig=N_{cover},1} Q^{th}_{d_{j=N_x}} + G^{so}_{ig=N_{cover},1} Q^{so}_{d_{j=N_x}} - Q^l_{cv_{ig=N_{cover}}}$$

$$+ \quad \frac{K_g A_b}{D_x}(T_{g_{ig=N_{cover},j=2}} - T_{g_{ig=N_{cover},j=1}})]/(M_g Cp_g(\frac{1}{N_x}))$$

For uppermost strip i.e. $j = N_x$.

$$\frac{\Delta T_{g_{ig=N_{cover},j=N_x}}}{\Delta t} = [Q^p_{abs_{ig=N_{cover},j=N_x}} + Q^s_{abs_{ig=N_{cover},j=N_x}} - \Delta E_{ig=N_{cover},j=N_x} \tag{104}$$

$$+ \quad Q^{sb}_{in_{ig=N_{cover},b}} Q^d_{sb_{j=N_x}} \tau^{mix^{so}}_{ig-1,16} + G^{th}_{ig=N_{cover}-1,5} Q^{th}_{d_{j=N_x}} + G^{so}_{ig=N_{cover}-1,5} Q^{so}_{d_{j=N_x}}$$

$$+ \quad G^{th}_{ig=N_{cover},1} Q^{th}_{d_{j=1}} + G^{so}_{ig=N_{cover},1} Q^{so}_{d_{j=1}} - Q^u_{cv_{ig=N_{cover}}}$$

$$+ \quad \frac{K_g A_b}{D_x}(T_{g_{ig=N_{cover},j=N_x-1}} - T_{g_{ig=N_{cover},j=N_x}})]/(M_g Cp_g(\frac{1}{N_x}))$$

For intermediate strips i.e. $j = 2$ to $j = N_x - 1$.

$$\frac{\Delta T_{g_{ig=N_{cover},j}}}{\Delta t} = [Q^p_{abs_{ig=N_{cover},j}} + Q^s_{abs_{ig=N_{cover},j}} - \Delta E_{ig=N_{cover},j} \tag{105}$$

$$+ \quad Q^{sb}_{in_{ig=N_{cover},b}} Q^{sb}_{d_j} \tau^{mix^{so}}_{N_{cover},16} + G^{th}_{ig=N_{cover}-1,5} Q^{th}_{d_j} + G^{so}_{ig=N_{cover}-1,5} Q^{so}_{d_j}$$

$$+ \quad G^{th}_{ig=N_{cover},1} Q^{th}_{d_{j=(N_x+1-j)}} + G^{so}_{ig=N_{cover},1} Q^{so}_{d_{j=(N_x+1-j)}}$$

$$+ \quad \frac{K_g A_b}{D_x}(T_{g_{ig=N_{cover},j+1}} - 2T_{g_{ig=N_{cover},j}} + T_{g_{ig=N_{cover},j-1}})]/(M_g Cp_g(\frac{1}{N_x}))$$

For intermediate glass covers

Different radiations falling on the intermediate covers have been shown in Figure 14 .
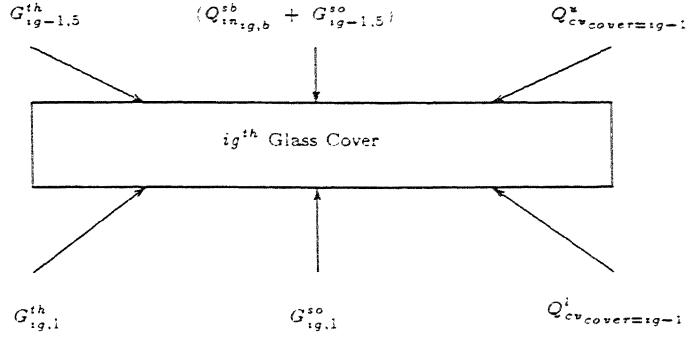
Figure 14: Incident Radiations on Intermediate Glass sheet When Multiple Covers

For lowermost strip i.e. $j = 1$.

$$
\begin{aligned}
\frac{\Delta T_{g_{ig,j=1}}}{\Delta t} = {} & [Q^p_{abs_{ig,j=1}} + Q^s_{abs_{ig,j=1}} - \Delta E_{ig,j=1} + Q^{sb}_{in_{ig,b}} Q^{sb}_{d_{j=1}} \tau^{mix^{so}}_{N_{cover},16} \qquad (106) \\
& + G^{th}_{ig-1,5} Q^{th}_{d_{j=1}} + G^{so}_{ig-1,5} Q^{so}_{d_{j=1}} + G^{th}_{ig,1} Q^{th}_{d_{j=N_x}} + G^{so}_{ig,1} Q^{so}_{d_{j=N_x}} - Q^l_{cv_{ig}} \\
& + \frac{K_g A_b}{D_x}(T_{g_{ig,j=2}} - T_{g_{ig,j=1}})]/(M_g Cp_g(\frac{1}{N_x}))
\end{aligned}
$$

For uppermost strip i.e. $j = N_x$,

$$
\begin{aligned}
\frac{\Delta T_{g_{ig,j=N_x}}}{\Delta t} = {} & [Q^p_{abs_{ig,j=N_x}} + Q^s_{abs_{ig,j=N_x}} - \Delta E_{ig,j=N_x} + Q^{sb}_{in_{ig,b}} Q^{sb}_{d_{j=N_x}} \tau^{mix^{so}}_{1,16} \quad (107) \\
& + G^{th}_{ig-1,5} Q^{th}_{d_{j=N_x}} + G^{so}_{ig-1,5} Q^{so}_{d_{j=N_x}} + G^{th}_{ig,1} Q^{th}_{d_{j=1}} + G^{so}_{ig,1} Q^{so}_{d_{j=1}} \\
& - Q^u_{cv_{ig}} + \frac{K_g A_b}{D_x}(T_{g_{ig,j=N_x-1}} - T_{g_{ig,j=N_x}})]/(M_g Cp_g(\frac{1}{N_x}))
\end{aligned}
$$

For intermediate strips i.e. $j = 2$ to $j = N_x - 1$.

$$
\frac{\Delta T_{g_{ig,j}}}{\Delta t} = [Q^p_{abs_{ig,j}} + Q^s_{abs_{ig,j}} - \Delta E_{ig,j} + Q^{sb}_{in_{ig,b}} Q^{sb}_{d_j} \tau^{mix^{so}}_{1,16} \qquad (108)
$$

$$+ \quad G^{th}_{ig-1.5} Q^{th}_{d_j} + G^{so}_{ig-1.5} Q^{so}_{d_j} + G^{th}_{ig.1} Q^{th}_{d_{j=(N_x+1-j)}} + G^{so}_{ig.1} Q^{so}_{d_{j=(N_x+1-j)}}$$

$$+ \quad \frac{K_g A_b}{D_x} (T_{g,g,j+1} - 2T_{g,g,j} + T_{g,g,j-1})]/(M_g C p_g (\frac{1}{N_x}))$$

$$(109)$$

4.7.5 Stability Condition

In the above equations. choice of Δx and Δt are not independent of each other. For the stability of the solution,coefficient of the $T_{g,g,j}$ must be positive.

For 1st strip and N_x^{th} strip. the stability criteria requires :

$$\frac{(\Delta x)^2}{\Delta t} > \frac{K_g A_b L_g}{M_g C p_g} \tag{110}$$

For intermediate strips. the stability criteria requires :

$$\frac{(\Delta x)^2}{\Delta t} > 2 \frac{K_g A_b L_g}{M_g C p_g} \tag{111}$$

4.8 Energy Balance Equations for Walls and Gas-mixture

4.8.1 FOR BOX

The temperature of the walls and the gas mixture in the box, after time interval Δt can be obtained by doing Energy balance of the heat fluxes absorbed and emitted. For the walls of the box, these equations are as follows

$$\frac{\Delta T_{B,i}}{\Delta t} = \frac{\alpha_i^{th}G_{B,i}^{'th} + \alpha_i^{so}G_{B,i}^{'so}\epsilon_i A_i T_{B,i}^4 - Q_{cv_{B,i}} - Q_{fl_{B,i}}}{M_{B,i}Cp_{B,i}} \tag{112}$$

$$\text{for } i = 2,3,4,5,6$$

$$\frac{\Delta T_{B,mix}}{\Delta t} = [Q_{in_{B,l}}^{sb} + Q_{in_{B,r}}^{sb} + Q_{in_{B,b}}^{sb} + G_{B,T}^{'so} + G_{B,T}^{'th}$$

$$- (\alpha_g^{so} + \tau_g^{so})G_{B,1}^{'so} - \sum_{j=2}^{6}\alpha_j^{so}G_{B,j}^{'so}$$

$$+ Q_{\tau_{N_{cover}}}^l - (\alpha_g^{th} + \tau_g^{th})G_{B,1}^{'th} + \sum_{j=2}^{6}\left(\epsilon_j A_j T_{B,j}^4 - \alpha_j^{th}G_{B,j}^{'th} + Q_{cv_{B,j}}\right)]/M_{B,mix}Cp_{B,mix}$$

4.8.2   FOR ig^{th} gap

Similarly, equations for increment in the temperatures of the walls and gas mixture in the gaps between the two glass covers can be calculated as

For ig^{th} gap,

$$\frac{\Delta T_{ig,i}}{\Delta t} = \frac{\alpha_{ig,i}^{th}G_{ig,i}^{th} + \alpha_{ig,i}^{so}G_{ig,i}^{'so}\epsilon_{ig,i}A_{ig,i}T_{ig,i}^4 - Q_{cv_{ig,i}} - Q_{fl_{ig,i}}}{M_{ig,i}Cp_{ig,i}} \tag{113}$$

$$\text{for } i = 2,3,4,5$$

$$\frac{\Delta T_{ig,mix}}{\Delta t} = [Q_{in_{ig,l}}^{sb} + Q_{in_{ig,r}}^{sb} + (\rho_g^{so} + \alpha_{ig,16}^{mix^{so}})Q_{in_{ig+1,b}}^{sb}$$

$$+ G_{ig,T}^{'so} + G_{ig,T}^{'th} + G_{ig,L}^{'so} + G_{ig,L}^{'th}$$

$$- (\alpha_g^{so} + \tau_g^{so})(G_{ig,1}^{'so} + G_{ig,6}^{'so}) - \sum_{j=2}^{5}\alpha_{ig,j}^{so}G_{ig,j}^{'so}$$

$$+ Q_{\tau_{ig}}^l + Q_{\tau_{ig+1}}^u - (\alpha_g^{th} + \tau_g^{th})(G_{ig,1}^{'th} + G_{ig,6}^{'th})$$

$$+ \sum_{j=2}^{5}\left(\epsilon_{ig,j}A_{ig,j}T_{ig,j}^4 - \alpha_{ig,j}^{th}G_{ig,j}^{'th} + Q_{cv_{ig,j}}\right)]/M_{ig,mix}Cp_{ig,mix}$$

4.9 Front Heat Loss

The front heat loss consists of the following losses.

[1]- Convective heat loss from the glass surfaces to atmosphere.

[2]- Radiative heat loss from the glass sheet to atmosphere.

[3]- Reflection of incident solar radiation.

[4]- Transmission of the reflected solar radiation from the inside surface of the collector.

[5]- Transmission of the thermal radiation from the inside surfaces of the collector.

4.10 Efficiency

The efficiency has been defined as the ratio of the total heat collected by the heat extracting or working fluid to the total incident beam and diffuse solar radiation on the outer glass sheet.

$$\eta = \frac{Total\ Heat\ Transferred\ To\ Working\ Fluid}{Q_{in_{1,b}}^{sb} + Q_{in}^{sd}} \tag{114}$$

Chapter 5

Solution Procedure

Step [1] Read input data.

Step [2] Initialize Temperature data.

Step [3] Initialize emissivity, absorptivity of gas as zero.

Step [4] Calculate Shape factors and Geometric mean beam lengths.

Step [5] Calculate Transmissivity, reflectivity and absorptivity of the glass sheet for thermal, infrared, beam solar and diffuse solar radiation.

Step [6] Calculate stripwise absorption of thermal, Infrared, beam solar and diffusesolar radiation in glass sheet.

Step [7] Calculate properties of air at ambient temperature.

Step [8] Formulate matrix form of equation for the analysis of the glass sheets.

Step [9] IF (no gas in box and single cover) THEN

Step [10] Calculate solar energy falling on different walls.

Step [11] Calculate solar irradiation on different walls of the box.

     GOTO Step [19].

Step [12] IF (no gas in box and gap) THEN

Step [13] Calculate the solar irradiation on walls of different gaps.

Step [14] Calculate solar irradiation on different walls of the box.

     GOTO Step [19].

Step [15] IF (gas in the box) THEN Calculate emissivity. absorptivity

     (for thermal and solar radiation both) of gas in box.

Step [16] IF (gas in the gap) THEN Calculate emissivity .absorptivity

     (for thermal and solar radiation both) of gas in gap.

Step [17] Calculate solar energy falling on different walls.

Step [18] Calculate solar irradiation on different walls of the box and

     gaps.

Step [19] Calculate heat transferred to the fluid.

Step [20] Calculate heat radiated by the glass sheets.

Step [21] Calculate secondary absorbed energy in glass sheets.

Step [22] Calculate convective heat transfer from different walls of box

     and covers.

Step [23] Calculate thermal irradiation on different walls of box and

     covers.

Step [24] Calculate temperature rise in different strips of glass sheets.

Step [25] Calculate temperature rise in different walls of box and gaps.

Step [26] Check time passed. IF (time < duration) GOTO Step [15] ELSE

     GOTO Step [27].

Chapter 6

Experimental set-up

6.1   Description

Main components of the solar collector. fabricated in the lab for conducting experiment.

are :

(1) Absorber plate

(2) Flow passage

(3) Glass Cover

(4) Insulation

(5) Containing box or casing

(6) Gas mixture used in the box

6.1.1   Absorber plate

The absorber plate is fabricated from 24 gauge copper sheet. The choice of copper

is based on high thermal conductivity to validate the assumption of uniform absorber

plate temperature. The absorber plates form a rectangular cavity with total five number of absorber plates. The sheets are blackned on the face receiving solar radiation. Black oxide is sprayed on the sheets to increase the solar absorptivity of the absorber plates.

6.1.2 Flow passage

The flow passage consists of rectangular channels of G.I. sheet, attatched to the side absorber plates in a spiral fashion, with two different flow paths. Selection of two flow paths is based on the requirement to extract the maximum amount of heat and to keep the side absorber plate temperatures approximately same for all four plates. The channels are attatched to the base in the same manner, so that flow leaves the absorber plate at the centre of the base absorber plate. This is done to extract the maximum amount of heat, because the centre is expected to be free from corner effects and to have the maximum temperature. Thus, it has been tried to keep the difference between the absorber plate and fluid temperature minimum and the fluid should come into contact with the wall at progressively higher temperatures.

6.1.3 Glass Cover

The experimental set-up is fitted with two number of glass sheets of thickness 4mm. The thickness is chosen as a compromise between the strength of the sheet and the heat loss. The gap between the two glass sheets is kept 1 inch. As the gap thickness is increased, the total heat losses are increased, hence the gap is kept at the minimum but with keeping the fabrication difficulties in mind. Rubber beading and packing

# :hes of the fabricated Solar Collector

w from Top
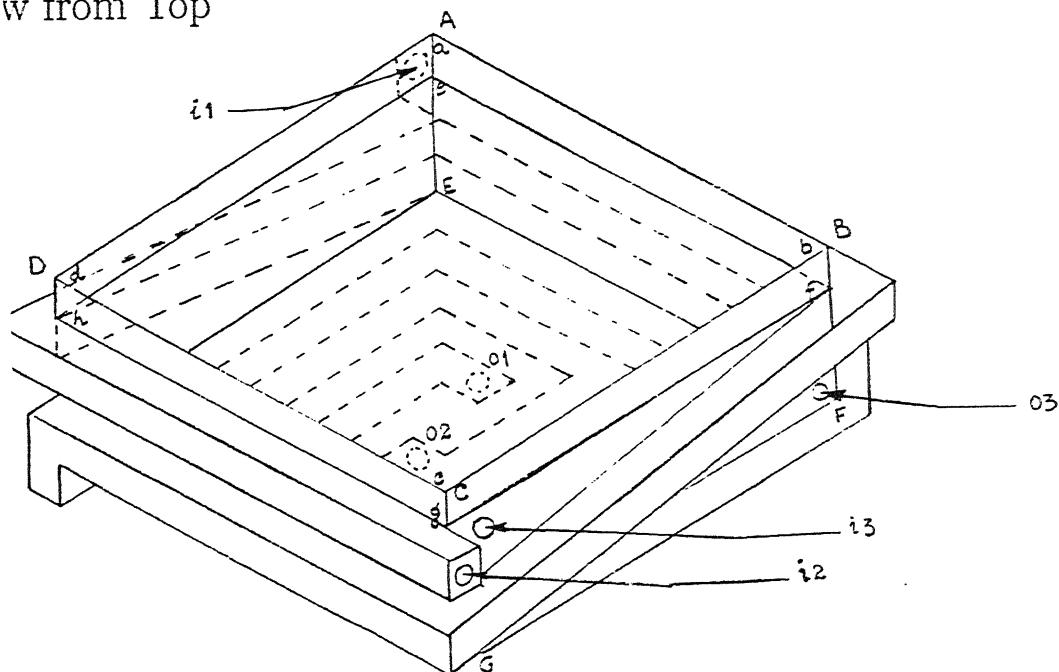
i1 : Fluid inlet 1
i2 : Fluid inlet 2
i3 : Gas inlet
o1 : Fluid outlet 1
o2 : Fluid outlet 2
o3 : Gas outlet
abcd : Outer glass cover
efgh : Inner glass cover
ABCDEFGH : Collector Box

Collector is shown without casing

w from Bottom
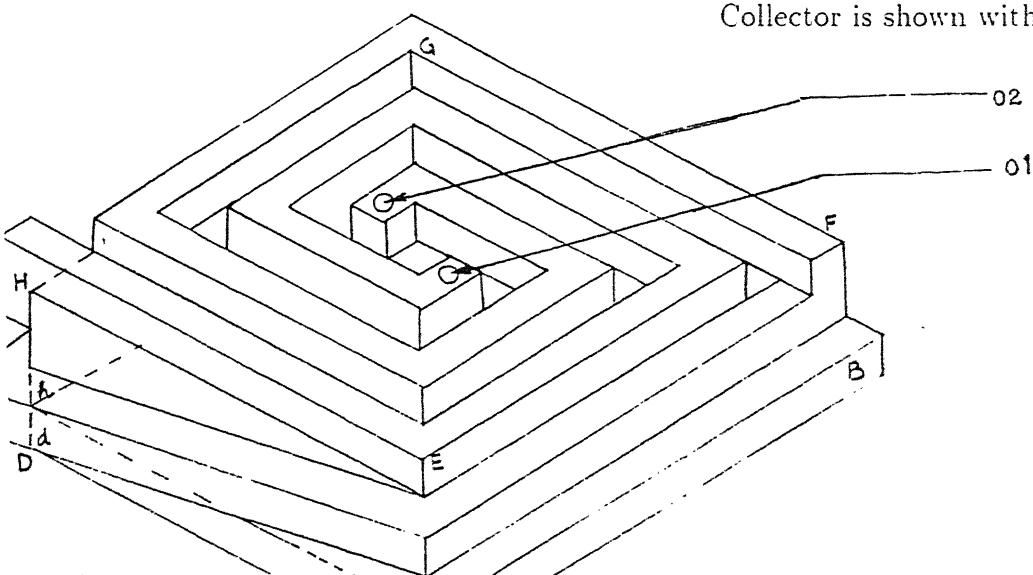
rubber sheet are used to make the gap air tight. Properties of different possible cover materials are given in all Solar Energy Handbooks [13].

6.1.4 Insulation

Glass wool insulation is used to insulate the flow channels in order to reduce the heat losses from side and base through the casing walls. Glass wool is selected because it can easily withstand temperatures of the order of $200 - 300\ °C$.

6.1.5 Containing box or casing

The absorber plates fitted with flow channels and insulated with Glass wool is kept in the G.I. casing of rectangular shape. The selection of the G.I. sheet is based on the strength and heat loss considerations.

6.1.6 Gas mixture used in the box

Ammonia gas is filled in the box. For filling and evacuating purpose two passage have been given. The lower passage is used for filling purpose whereas upper passage is used for evacuating. During filling, liquid ammonia is put in the box through the lower passage and upper passage is kept lock, air being heavier than ammonia, leaves out from the lower passage. The exact composition of the gas is difficult to measured, but an approximate can be made easily. To evacuate the gas mixture from the box, both passages are kept open, resulting in the leaving out of the gas-mixture through the upper passage and entering of fresh air from the lower passage.

6.1.7   Heat extracting fluid used

Depending upon the range of temperatures in operation. different fluids can be used for this purpose. Heat transfer fluids along with their density. specific heat and boiling point. heat transfer coefficient parameters are given in [30]. For the temperatures below 100 $^{\circ}C$. water is the best suited collector fluid.

6.2   Solar radiation Intensity Measurement

Solar radiation intensity on horizontal surface was measured using a Kipps and Zonen CM5 pyranometer (See Appendix C.Figure 36   ). It was put near to the collector and leads were connected to the digital milivoltmeter. Thermo-emf generated was measured and converted into solar inntensity by multiplying it by the pyranometer constant.

Chapter 7

Results and Conclusions

7.1   INPUT DATA for Computation

[1]. Geometric parameters :

$L_a = L_b = 60.0$ cm.

$L_c = 15.0$ cm.

$\Delta_g = 4.0$ mm.

$\Delta_{gap} = 3.0$ cm.

$L_{cha} = 3.0$ cm.

$\beta = 40.0$ °

[2]. Optical properties of glass :

$\gamma_{th} = 8000.0\ m^{-1}$

$\gamma_{in} = 4400.0\ m^{-1}$

$\gamma_{so} = 30.0\ m^{-1}$

$n_{th} = 1.35$

n_{in}= 1.40

n_{so}= 1.52

[3]. Thermal properties of wall material :

K_{copper}= 386.0 $W/m - K$

$C_{p_{copper}}$= 386.02 $J/Kg. - K$

M_{copper}= 4.613 $Kg./m^2$

$\epsilon_{paintedcopper}$= 0.95

$\alpha^{so}_{paintedcopper}$= 0.98

$\alpha^{th}_{paintedcopper}$= 0.95

[4]. Thermal properties of Glass :

K_{glass}= 0.80 $W/m - K$

$C_{p_{glass}}$= 669.92 $J/Kg. - K$

M_{glass}= 10.000 $Kg./m^2$

[5]. Average Thermal properties of air :

$C_{p_{air}}$= 1004.88 $J/Kg. - K$

M_{air} = 1.1650 $Kg./m^3$

[6]. Average Thermal properties of NH_3 :

$C_{p_{NH_3}}$ = 2113.60 $J/Kg. - K$

M_{NH_3} = 0.6880 $Kg./m^3$

[7]. Solar parameters :

N_{day}= 115

$Lattitude$= 26.6 °

I_{sc}= 1353.0 W/m^2

K_T= 0.80

$$a(K_T) = 0.270$$

$$b(K_T) = 0.395$$

[8]. Ambient air parameters :

$$V_{air} = 3.00 \text{ m/s}$$

$$RH = 0.50$$

$$CC = 0.00$$

$$a(sky) = 0.6164$$

[9]. Modelling parameters :

$$N_x = 16$$

$$N_g = 180$$

$$\Delta t = 0.05$$

$$TimePeriod = 2 \text{ Hours (IST 11:00 to 13:00 Hours)}$$

7.2 Computational Results for Nontracking collector

The computational results for the nontracking collector with the parameters listed in the above section, can be explained in two sections. first being the transient performance of the collector and the second the overall performance of the collector.

7.2.1 Transient Performance of Nontracking Collectors

For the study of the effect of the absorbing media on the transient performance of the collector, results have been computed for partial pressure of $NH_3 = 0.0, 0.4, 0.8, 1.0$
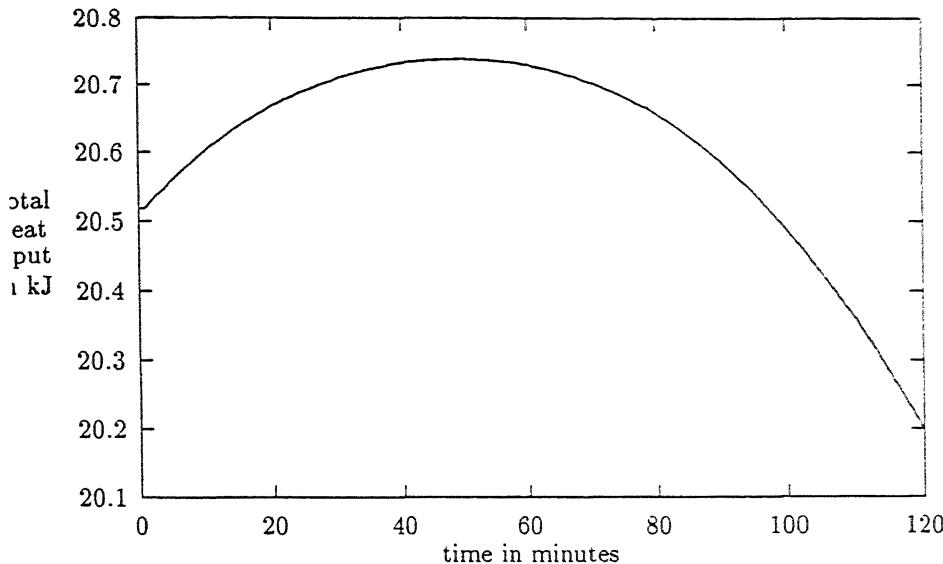
Figure 15: Nontracking : Variation of Input Solar Energy with time
(on the base plate)

and evacuated case with no selective coating. The results have been computed for the

fixed geometry of the collector and water flow rate.

$L_a = L_b = 60.0$ cm.

$L_c = 15.0$ cm.

$L_{gap} = 3.0$ cm.

$V_w = 0.005$ m/s

7.2.1.1   Variation of Input Solar Energy with time

Input solar energy   consists of two parts. diffuse and beam solar radiation. The beam

component is proportional to the cosine of the incidence angle of the falling radiation.

The incidence angle varies with the hour angle according to Equation 3 . The diffuse

component depends upon the hour angle because of the hour angle dependence of the

extra-terrestrial horizontal solar intensity. The variation of input solar energy with
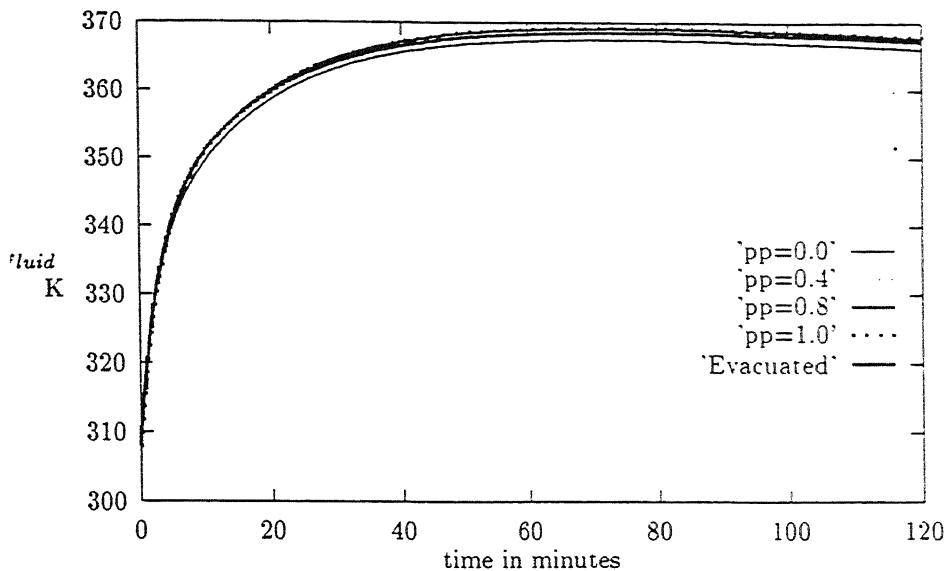
Figure 16: Nontracking : Variation of Working Fluid Outlet Temperature with time

time is shown in Figure 15 .

7.2.1.2 Variation of Working Fluid Outlet Temperature with time

The angle of incidence of the beam radiation changes from zero at solar noon to finite values for before and after solar noon. Thus the radiation falling on the base plate increases before the solar noon and starts decreasing after the solar noon, which results in the fluid outlet temperature rise before solar noon and fall after solar noon. The variation of fluid outlet temperature with time is shown in Figure 16 .

7.2.1.3 Variation of Outer Glass Temperature with time

The variation of the outer glass temperature depends on the solar and thermal radiation falling on it and optical properties of the glass. Since the use of the NH_3 reduces the thermal flux on the glass sheet, its temperature is reduced with increasing partial

T_{cover} in K
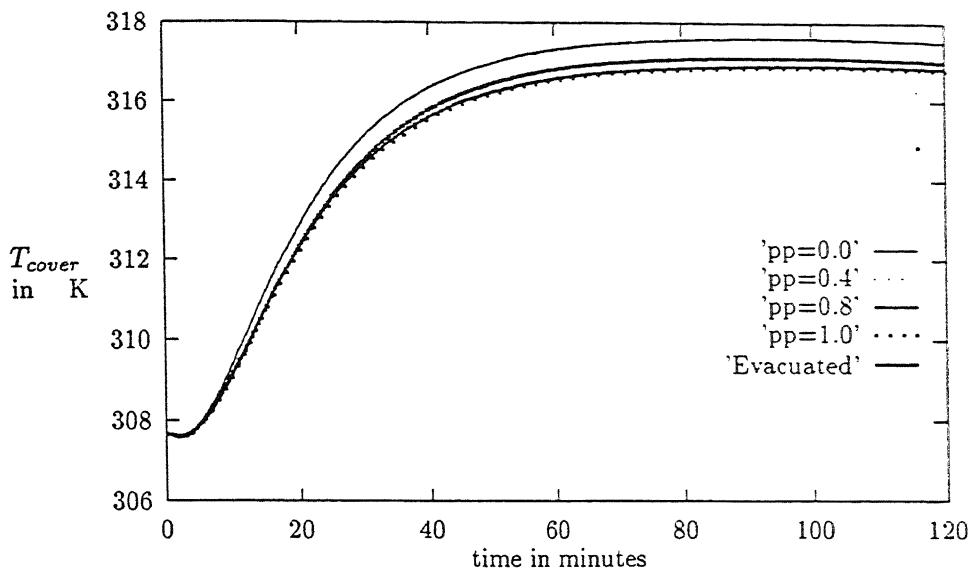
Figure 17: Nontracking : Variation of Outer Glass Temperature with time

pressure. The variation of Outer glass temperature with time is shown in Figure 17 .

7.2.1.4 Variation of Front Heat Loss with time

Front heat loss consists of two components, first is the radiative loss from the outer side of the glass sheet and second is the convective heat loss from the outer side of the glass sheet. The convective heat loss coefficient strongly depends upon the wind velocity. The variation of front heat loss with time is shown in Figure 18 .

7.2.1.5 Variation of Heat Extracted by Working Fluid with time

The amount of heat collected is directly proportional to the incoming energy. Thus the trend of this curve is similar to that of the total input solar energy. The variation of heat extracted by working fluid with time is shown in Figure 19 .
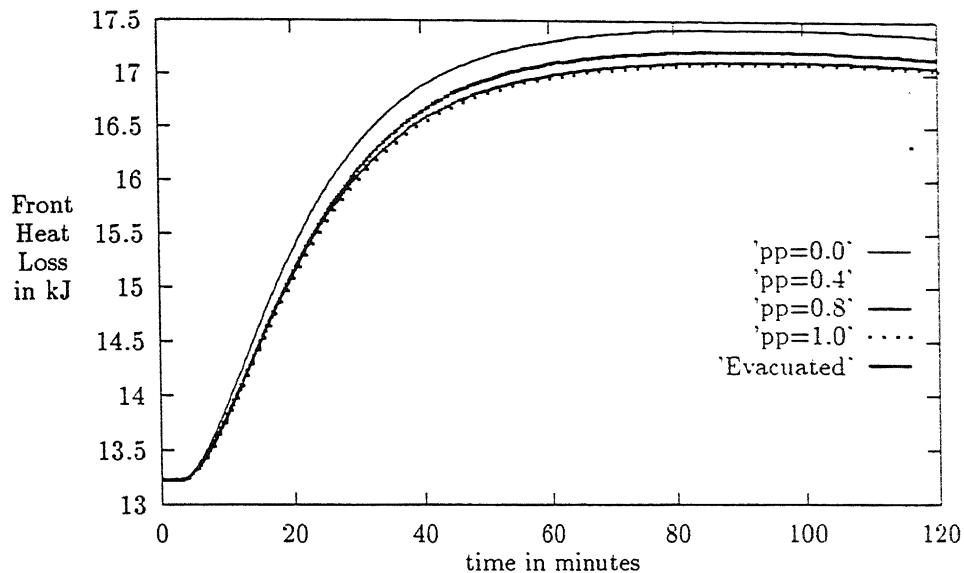
Figure 18: Nontracking : Variation of Front Heat Loss with time
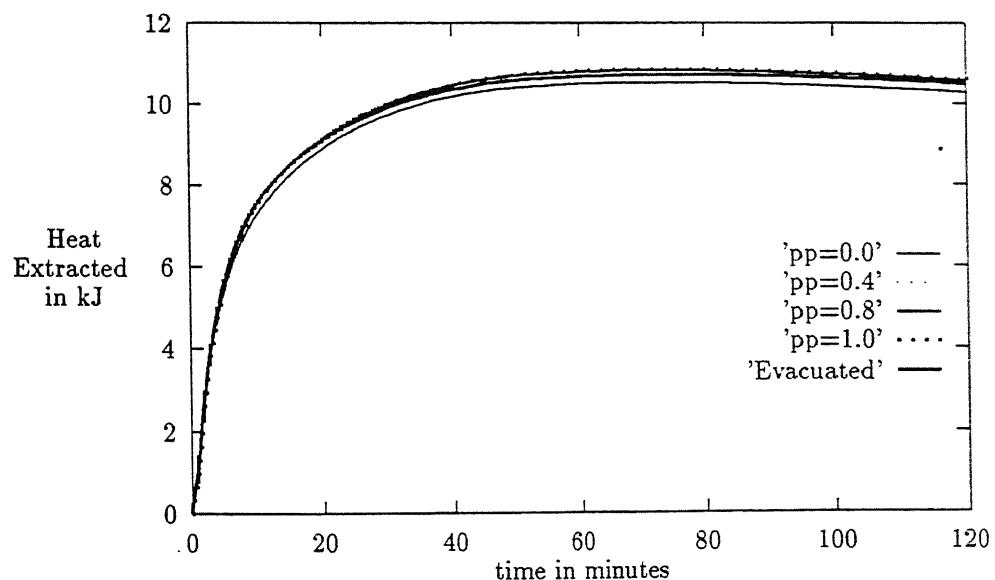
Figure 19: Nontracking : Variation of Heat Extracted by Working Fluid with time
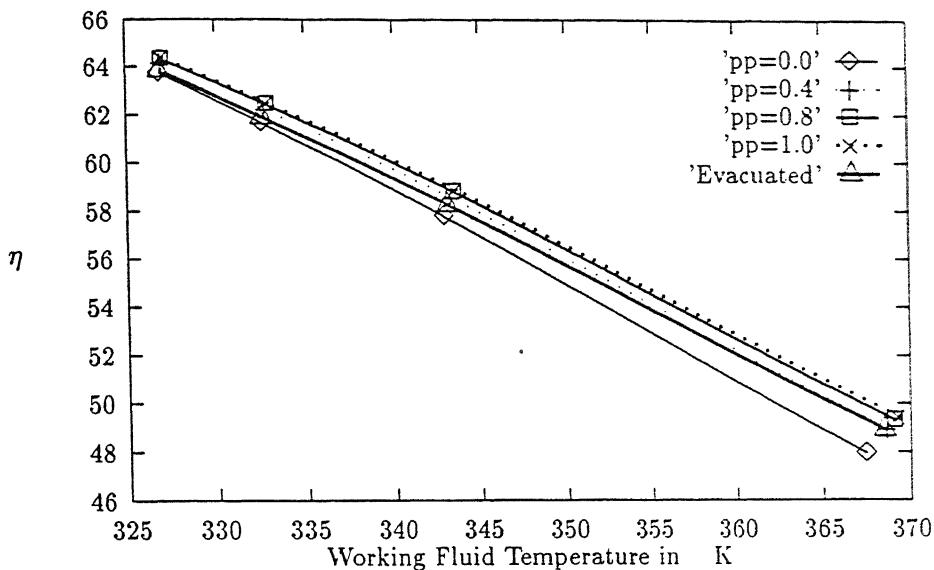
Figure 20: Nontracking: Collection Efficiency vs Fluid outlet temperature

7.2.2 Overall Performance of Nontracking Collectors

For the study of the effect of the absorbing media on the overall performance of the collector, results have been computed for partial pressure of $NH_3 = 0.0$. 0.4. 0.8. 1.0 and evacuated case with no selective coating. The results have been computed for the fixed geometry of the collector and different water flow rates.

7.2.2.1 Variation of Collection Efficiency with Fluid outlet temperature

The plot of the η vs $T_{fl_{out}}$, Figure 20, for various partial pressure of the gas in the collector box, clearly indicates that the use of the absorbing media i.e. NH_3 increases the collection efficiency by fairly good percentage as compared to the air filled collector at high temperatures. At lower temperature the temperature of the absorber plate (base) is not very high, giving the case of enclosure with uniform wall temperatures.
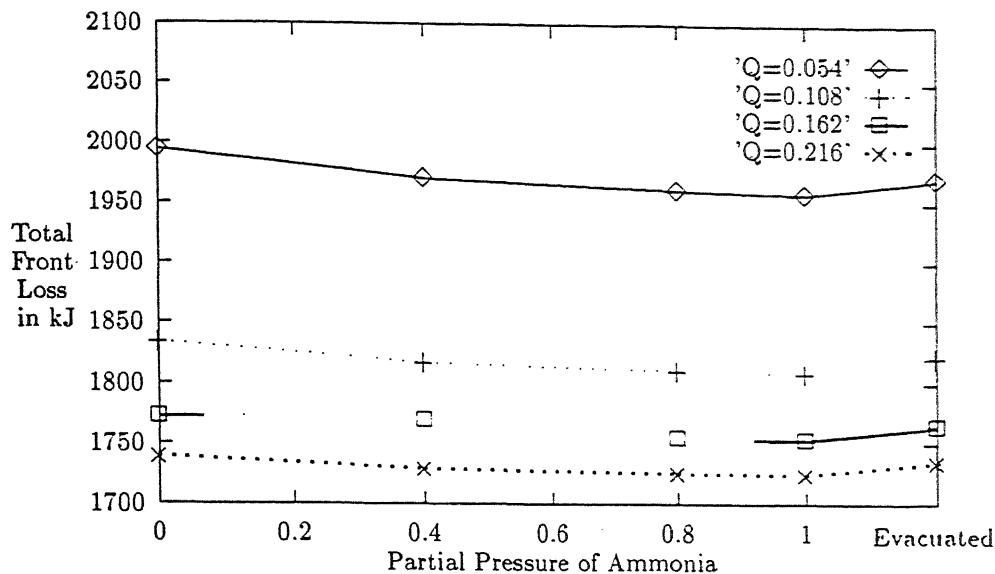
Figure 21: Nontracking : Total Front Heat Loss vs Partial pressure of NH_3

Thus radiation flux falling on all sides of the box are nearly same, resulting in marginal gain in the efficiency. The use of the absorbing media cuts down the high intensity radiation flux on the glass sheet from the inner side (due to higher temperature of the base plate) to the glass sheet by absorbing it and then re-emits it uniformly in all directions, causing a reduction in the thermal flux on the glass sheet from inner side.

The variation of the increase in the efficiency with partial pressure depends upon the emissivity and the absorptivity of the gas. It increases with partial pressure of NH_3, at faster rate in the starting and becomes almost constant at higher values.

7.2.2.2   Variation of Total Front Heat Loss with partial pressure of NH_3

The total front heat loss decreases with increasing partial pressure. But the difference in the values becomes smaller and smaller with increasing flow rates, i.e. at lower fluid outlet temperatures. This happens because at lower absorber plate temperature both
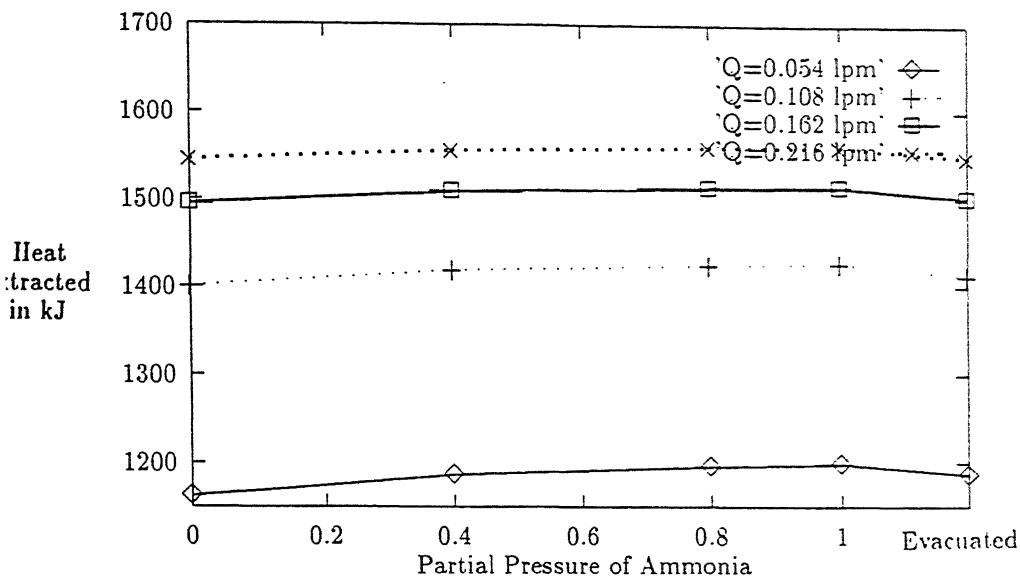
Figure 22: Nontracking : Total Heat Extracted by Working Fluid vs Partial pressure of NH_3

the glass sheet and the absorber plate is at nearly same temperature. which makes the use of gas ineffective. The variation of total front heat loss with partial pressure of NH_3 is shown in Figure 21 .

7.2.2.3 Variation of Total Heat Extracted by Working Fluid with partial pressure of NH_3

The total heat extracted by working fluid increases with increasing partial pressure. But the difference in the values becomes smaller and smaller with increasing flow rates. because of the reason stated in the case of the total front heat loss. The variation of total heat extracted by working fluid with partial pressure of NH_3 is shown in Figure 22 .
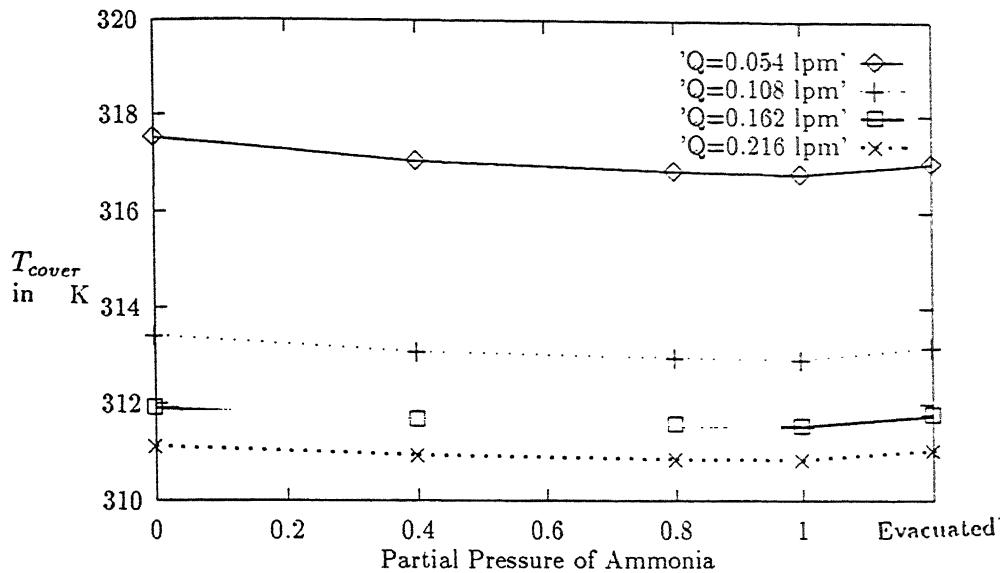
Figure 23: Nontracking : Outer Cover Temperature vs Partial pressure of NH_3

7.2.2.4 Variation of Outer Cover Temperature with partial pressure of NH_3

The outer cover temperature increases with increasing partial pressure. But the difference in the values becomes smaller and smaller with increasing flow rates. because of the reason stated in the case of the total front heat loss. The variation of outer cover temperature with partial pressure of NH_3 is shown in Figure 23 .

7.2.2.5 Variation of Working Fluid Outlet Temperature with partial pressure of NH_3

The variation of working fluid outlet temperature with partial pressure of NH_3 is shown in Figure 24 . It also shows the same behavior that, at lower temperatures there is only marginal gain in the outlet temperature whereas at higher outlet temperatures gain is sufficient.
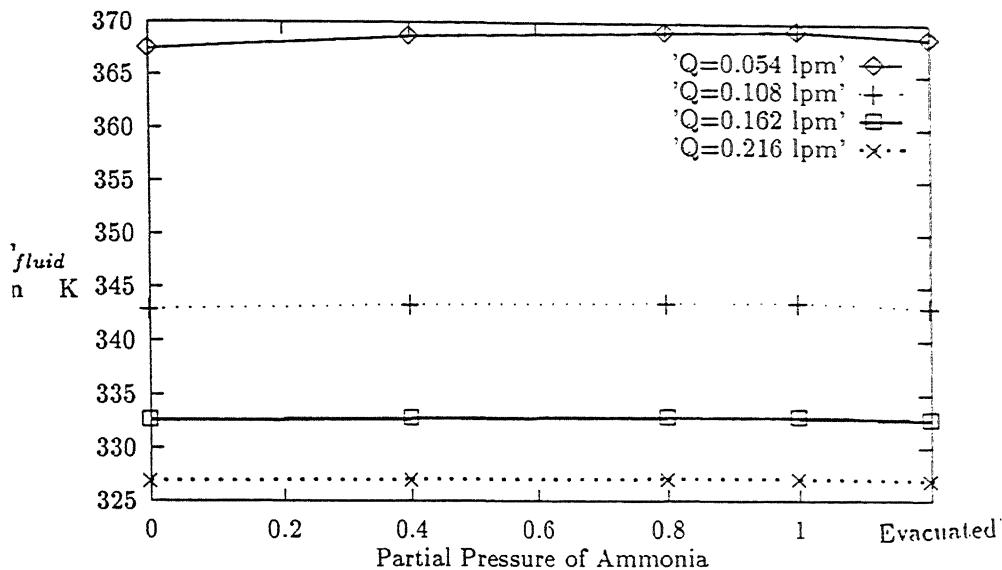
Figure 24: Nontracking : Working Fluid Outlet Temperature vs Partial pressure of NH_3

7.3 Computational Results for Tracking Collector

The computational results for the tracking collector with the parameters listed in the above section are explained as follows. The incident beam radiation is constant in this case because of the tracking of the collector. Hence all quantities attain a steady state value after some period. Thus in the transient study values first increase rapidly and with the passage of the time they achieve steady state value.

7.3.1 Transient Performance of Tracking Collector

For the study of the effect of the absorbing media on the transient performance of the collector, results have been computed for partial pressure of $NH_3 = 0.0$, 0.4, 0.8, 1.0 and evacuated case with no selective coating. The results have been computed for the
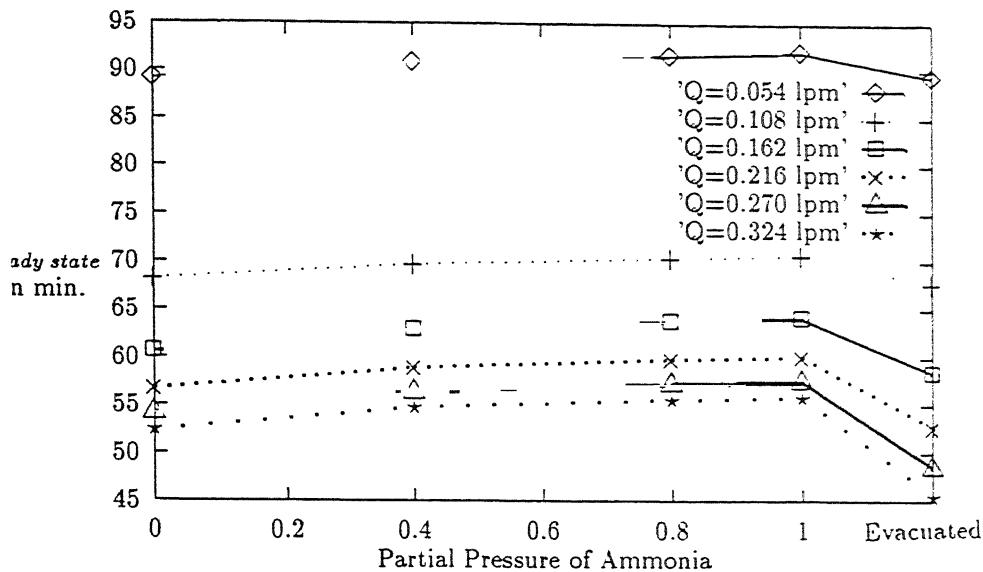
Figure 25: Tracking : Variation of Time for achieving steady state with Partial pressure of NH_3

fixed geometry of the collector and water flow rate.

7.3.1.1 Variation of Time for achieving steady state with Partial pressure of NH_3

The variation of time required to attain the steady state by the collector with partial pressure of NH_3 is shown in Figure 25 . Time taken by the collector to achieve the steady state is least in the case of the evacuation and it increases with the partial pressure of the NH_3, because the gas itself starts taking active part in energy transfer.

The values of the front heat loss. heat transferred to the working fluid. working fluid outlet temperature and the outer glass temperature at the steady state had been plotted and they show the same trend as in the case of nontracking collectors.
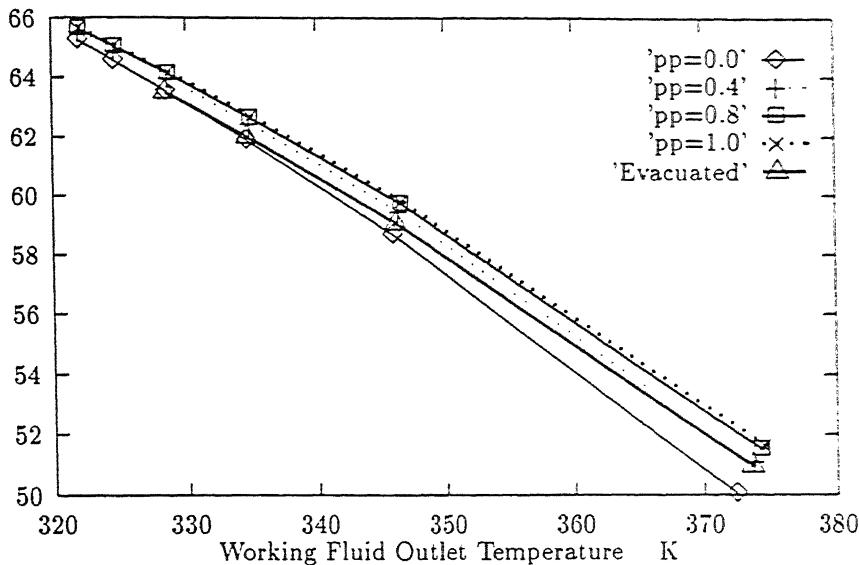
Figure 26: Tracking : Collection Efficiency vs Fluid Outlet Temperature

7.3.2 Overall Performance Of Tracking Collector at steady state

For the study of the effect of the absorbing media on the overall performance of the collector, results have been computed for partial pressure of $NH_3 = 0.0, 0.4, 0.8, 1.0$ and evacuated case with no selective coating. The results have been computed for the fixed geometry of the collector and different water flow rates.

The plot of the η vs $T_{fl_{out}}$, Figure 26 , for various partial pressure of the gas in the collector box, clearly indicates that the use of the absorbing media i.e. NH_3 increases the collection efficiency by fairly good percentage as compared to the air filled collector at high temperatures. At lower temperature the temperature of the absorber plate (base) is not very high, giving the case of enclosure with uniform wall temperatures. Thus radiation flux falling on all sides of the box are nearly same. resulting in marginal
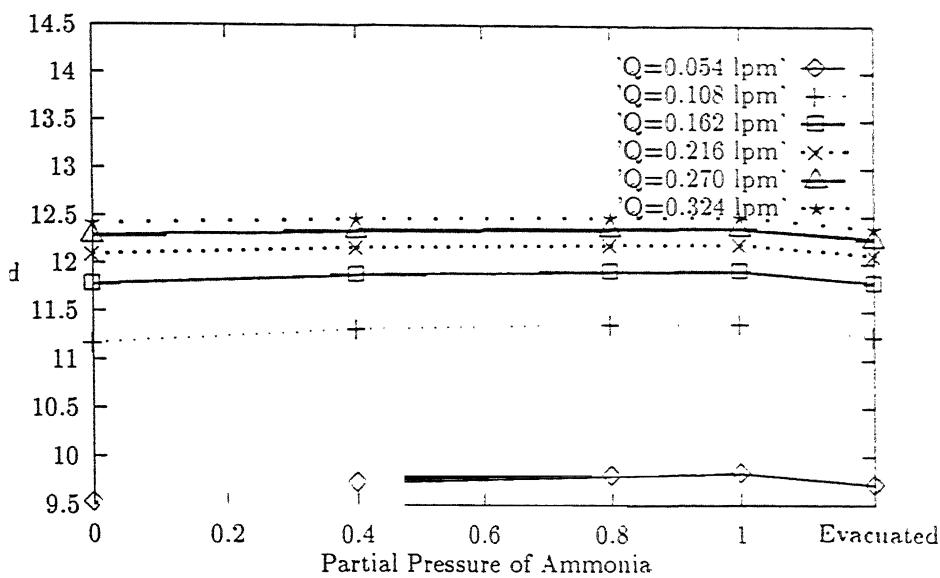
Figure 27: Tracking : Total Heat Extracted by Working Fluid vs Partial pressure of NH_3

gain in the efficiency. The use of the absorbing media cuts down the high intensity radiation flux on the glass sheet from the inner side (due to higher temperature of the base plate) to the glass sheet by absorbing it and then re-emits it uniformly in all directions. causing a reduction in the thermal flux on the glass sheet from inner side.

The variation of total heat extracted by working fluid with partial pressure of NH_3 is shown in Figure 27 .

The variation of total front heat loss with partial pressure of NH_3 is shown in Figure 28 .

The variation of outer cover temperature with partial pressure of NH_3 is shown in Figure 29 .

The variation of working fluid outlet temperature with partial pressure of NH_3 is shown in Figure 30 .
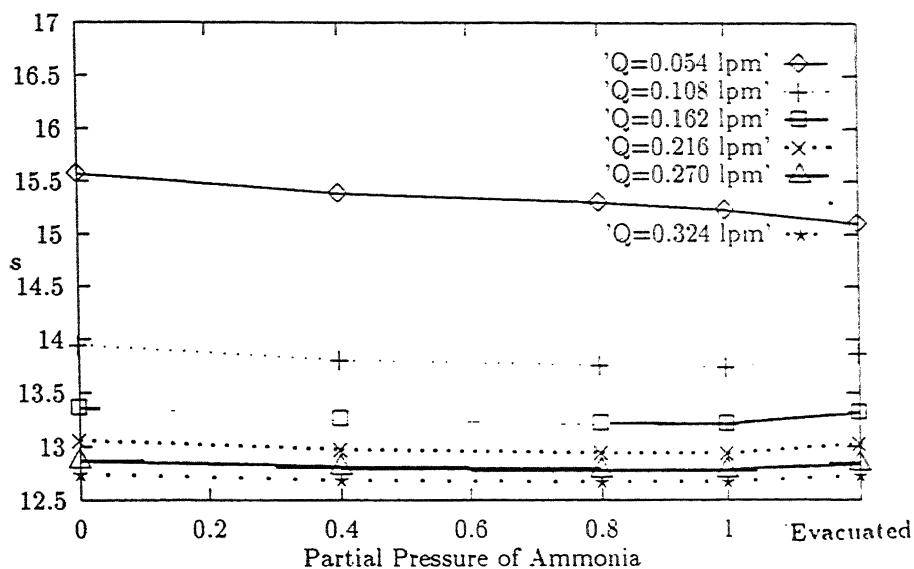
Figure 28: Tracking : Total Front Heat Loss vs Partial pressure of NH_3
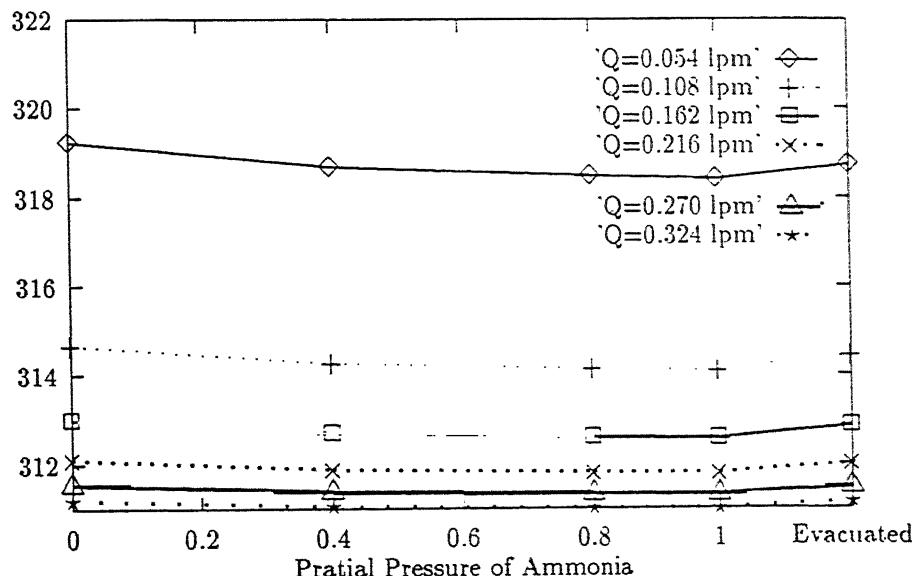
Figure 29: Tracking : Outer Cover Temperature vs Partial pressure of NH_3
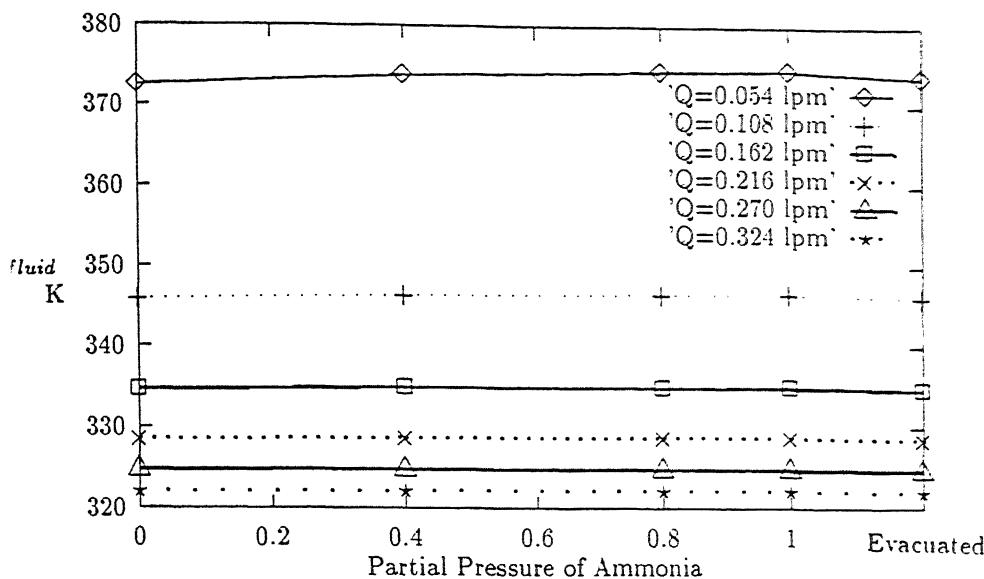
Figure 30: Tracking :Working Fluid Outlet Temperature vs Partial pressure of NH_3

The explanation of the above plots is the same as that given in the case of non-tracking collector.

7.4 Experimental Results

Experiments had been conducted for the polar tracking mode with gap between the cover and the absorber plate filled with air and gas respectively. The values of the solar intensity, ambient temperature and fluid inlet and outlet temperature and flow rate of the working fluid had been measured. Finally the collection efficiency had been calculated and plotted. Figure 31 , with outlet temperature. The plot show the same behavior as predicted by the computational results, but the values are not matching exactly. The main reasons for the difference in the values lies with the optical properties of the glass, convective heat transfer in the channel and variation in
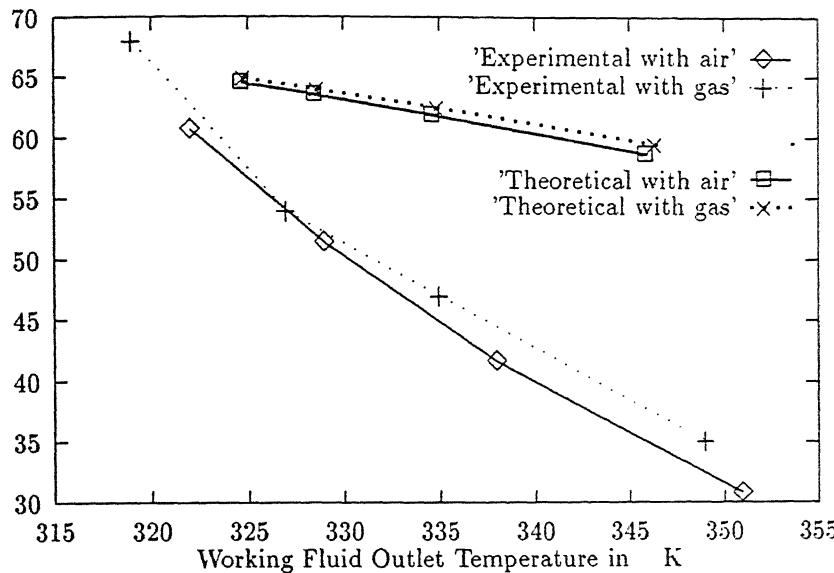
igure 31: Experimental Results: Collection Efficiency vs Fluid Outlet Temperature

ambient conditions.

.5 Effect of Gap between Glass Sheets on Collector Performance

the distance between the two glass sheets is increased, less thermal radiation reaches

the outer glass sheet, because the side walls also starts coming into picture by

eiving some amount of the radiation emitted by the lower glass sheet. At the same

ie in the case of the nontracking collector, the side walls starts intercepting the solar

liation, thereby, reducing the total solar energy input to the absorber plate. This

1 be avoided if the channels are attatched to the side walls starting from the top, i.e.

ter also extract heat from the space between the two glass sheets. In the present
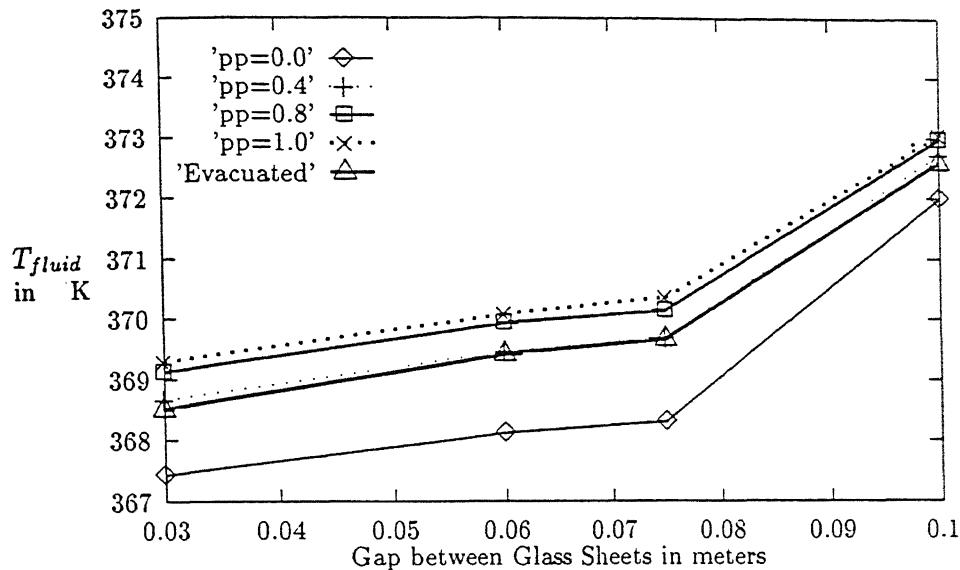
Figure 32: Nontracking : Working Fluid Outlet Temperature vs Gap

case the analysis as well as experimental set up uses this configuration. If the gas is used in the gap also, the increase in the gap causes more absorption of the thermal radiation and reduced emission towards the outer glass sheet because of the reduced configuration factor.

These factors result in the overall increase in the efficiency and the outlet temperature of the working fluid. The increase in the efficiency is increasing with gap distance initially and starts decreasing when the gap distance is too much. The computational results have been plotted for both the cases, nontracking, Figure 32 , 34 , and tracking, Figure 33 , 35 .
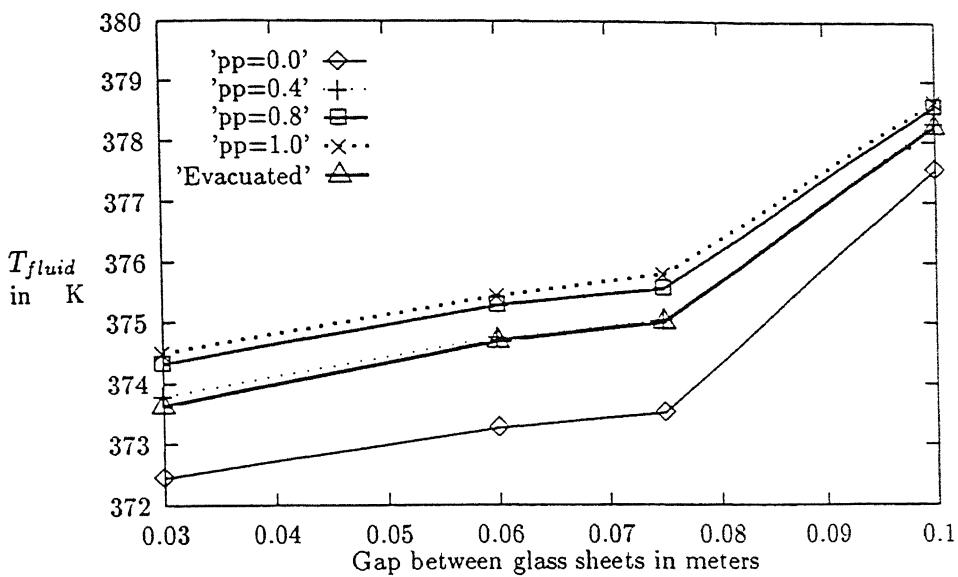
Figure 33: Tracking : Working Fluid outlet Temperature vs Gap
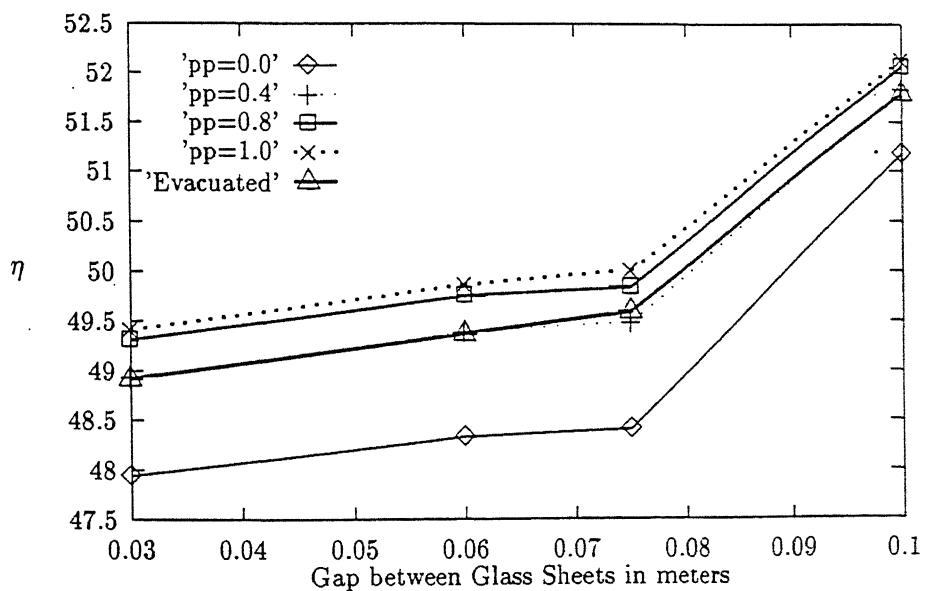
Figure 34: Nontracking : Heat Collection Efficiency vs Gap
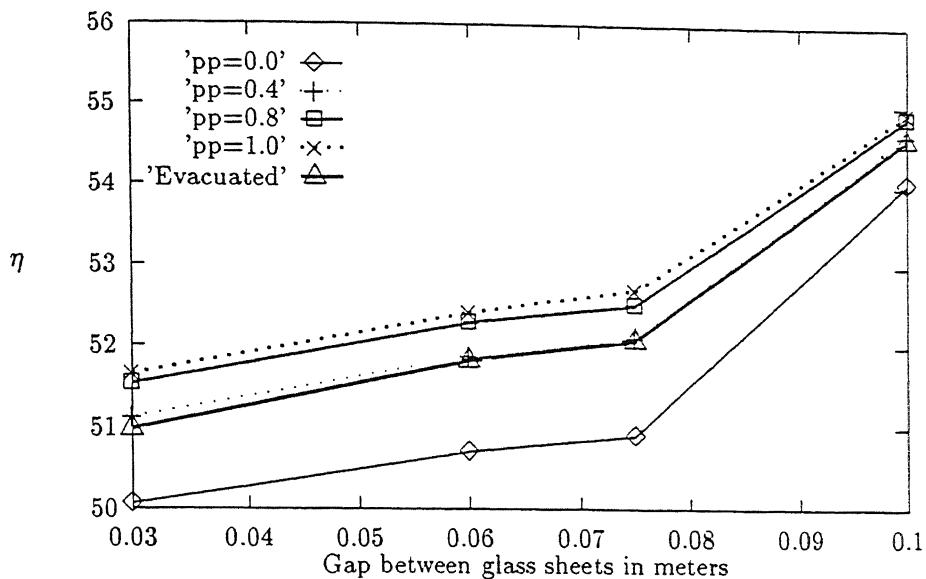
Figure 35: Tracking : Heat Collection Efficiency vs Gap

7.6   Conclusions

From the computational and experimental results, the following conclusions can be made :

[1] Use of the gases which are transparent for solar radiation and strongly absorbing and emitting for thermal radiation, can be helpful in improving the collector's performance.

[2] But their use is effective only at higher temperature applications. At lower temperatures, the improvement is not sufficient to be of practical importance.

[3] Use of the absorbing media can be helpful in improving the performance of the concentrating type of solar collectors, where absorber plate temperature is usually much higher than the glass cover temperature.

[4] Use of the absorbing media can also be helpful in improving the performance of

the nonconcentrating type of solar collectors, where reflector mirror is used to increase the intensity of solar radiation to achieve higher temperatures.

Table : Readings for collector with air in it :

low rate 1 lpm	$T_{ambient}$ °C	Heat input Watts	$T_{fluid_{inlet}}$ °C	$T_{fluid_{outlet}}$ °C	Heat Extracted Watts	Efficiency %
.167	42.0	325.56	32.0	49.0	197.71	60.70
.100	42.0	325.56	32.0	56.0	167.47	51.40
.059	42.0	325.56	32.0	63.0	135.46	41.60
.031	42.0	325.56	32.0	78.0	100.33	30.80

Table : Readings for collector with gas in it :

Flow rate n lpm	$T_{ambient}$ °C	Heat input Watts	$T_{fluid_{inlet}}$ °C	$T_{fluid_{outlet}}$ °C	Heat Extracted Watts	Efficiency %
0.222	41.0	319.30	33.0	46.0	217.10	68.00
0.117	41.0	319.30	33.0	54.0	172.40	54.00
0.074	41.0	319.30	33.0	62.0	149.90	47.00
0.036	41.0	319.30	33.0	76.0	112.15	35.10

Chapter 8

Suggestion for Further Study

- The study can be extended to concentrating type of collectors, where it is expected to give even better results.

- The study can be extended for other absorbing-emitting gases which are transparent for solar radiation and highly absorbing for thermal radiation.

- The study can be extended to include the effect of spectral emission of the gaseous media, because in the case of selective surface use of the Hottel's emissivity chart are not valid. Even for present case it is not very accurate.

- The absorber plate temperature had been assumed uniform throughout the plate, which is not strictly true. The effect of this can be studied by dividing the plate in number of zones. It will increase the computational complexity, but will give more accurate results.

Bibliography

[1] Edwards, D.K. "Radiation Interchange in A Nongray Enclosure Containing An Isothermal CO_2-N_2 Mixture." Journal of Heat Transfer, Trans ASME, Feb., 1962 Page [1-11]

[2] Edwards, D.K. and Nelson, K.E. "Rapid Calculation of Radiant Energy Transfer Between Nongray Walls and Isothermal H_2O or CO_2 Gas." Journal of Heat Transfer, Trans ASME, November, 1962 Page [273-278]

[3] Bevans, J.T., Dunkle R.V. "Radiation Interchange within Enclosure." Journal of Heat Transfer, Trans ASME, Series C, Volume 82, Feb., 1962 Page [1-9]

[4] Dunkle R.V. "Geometric Mean Beam Lengths for Radiation Heat Transfer Calculations." Journal of Heat Transfer, Trans ASME, Volume 86, No.1, 1964 page[75-80]

[5] Venkateawaran, S., Thynell, S.T. and Merkle, C.L. "A Study of Thermal Radiation Transfer in A Solar Thruster." Trans ASME Volume 113, November, 1991 page[932-937]

[6] Hottel, H.C., and Mangelsdorf, H.G. "Heat Transmission from Non-Luminious Gases -II Experimental Study of CO_2 and H_2O" Trans AIChE Volume 31. 1935 page[517]

[7] Hottel, H.C., and Cohen, E.S. "Radiant Heat Exchange in A Gas Filled Enclosure : Allowance for nonuniformity of Gas Temperature." Trans AIChE Volume 4. No.1, March, 1958 page[1-14]

[8] Hottel, H.C. and Sarofim, A.F. "Radiative Transfer." McGraw Hill Book Company, New York, 1967 Chapter [4,6]

[9] Seigel, R. and Howell, J.R. "Thermal Radiation Heat Transfer." McGraw Hill Book Company, New York, 1972 Chapter [4,13,17]

[10] Weibett, J.A. "Engineering Radiation Heat Transfer", Holt, Rinehart and Winston, New York, 1966. Chapter [7]

[11] Henry Blau and Heinz Fischer "Radiative Transfer from Solid Materials." The Macmillan Company, New York, 1962 Page [8-24]

[12] Kreider, Jan F. "Medium and High Temperature Solar Processes." Academic Press, New York, 1979. Chapter [2]

[13] Kreider, Jan F. "Solar Energy Handbook." Academic Press, New York, 1979. Chapter [2]

[14] Ari Rabl "Active Solar Collectors and Their Applications" Oxford University Press, New York, 1985.

[15] David K. McDaniels "The Sun" John Wiley and Sons, New York, 1984.

[16] Anderson, Edward E. "Fundamentals of Solar Energy Conversion" Addison Wesley Publishing Company, 1982. Chapter [1,2,3,5,6]

[17] Sparrow, E.M. and Cess, R.D. "Radiative Heat Transfer" McGraw Hill Book Company, New York, 1978 Chapter [1]

[18] Holman, J.P. "Heat Transfer." McGraw Hill International Book Company, New York, 1972.

[19] "American Institute of Physics Handbook." McGraw Hill Book Company, New York, 1963.

[20] McAdams, W. H. "Heat Transmission" Asian Student's Edition. McGraw Hill Book Company, New York, 1954

[21] Chapman, A.J. "Heat Transfer." Macmillon Publishing Company, New York, 1984.

[22] Lienhard, J.H. "A Text Book of Heat Transfer." Prentice Hall, 1987.

[23] ASHRAE Handbook and Products Directory, Fundamentals Volume. ASHRAE 1977

[24] Rich, B.R., "An Investigation of Heat Transfer from An Inclined Flate Plate in Free Convection." TRANS ASME Volume 75, 1953 page[489-499]

[25] Fujii, T. and Imura, H. "Natural Convection Heat Transfer from A Plate with Arbitrary Inclination." International Journal Heat Mass Transfer 1972. Volume 15 page[755]

[26] Goldstein, R.J., Sparrow, E.M. and Jones, D.C. "Natural Convection Heat mass Transfer Adjacent To The Horizonal Plates." International Journal Heat Mass Transfer 1973, Volume 16 page[1025]

[27] Churchill, S.W. and Chu, H.H.S. "Correlating Equations for Laminar and Turbulent Free Convection from Vertical plates." International Journal Heat Mass Transfer 1975, Volume 16 page[1323]

[28] Collins and Robinson "Evacuated Glazing" Journal Solar Energy. Volume 47. 1991

[29] Robert L. Pirog and Stephen C. Stamos "Energy Economics : Theory and Policies" Printice Hall, New Jersey, 1987.

[30] Jasbir Singh "Heat Transfer Fluids and Systems for Processes and Energy Applications", New York, Marcel Dekker, 1985.

[31] Ashok V. Desai "Nonconventional Energy" Wiley Eastern Limited. New Delhi. 1990.

[32] "Comparison of The Thermal Performance of Flat Plate and Evacuated Tubular Collectors." "Advances in Solar Energy Technology" Edited by Bloss W.H. and Pfisterer, F. Proceedings of the Biennial Congress of international Solar Energy Society, Hamburg, 1987

[33] Chandra K. S. "Optimum Tilt Angle for Flat Plate Solar Collector for Maximum Natural Flow" M.Tech. Thesis, I.I.T.,Kanpur.

Appendix: A

Tables Related to Solar Intensity Calculations [28].

Table 9: Coefficients $a(K_T)$ and $b(K_T)$ for Beam Radiation Model

Interval for k_T	$a(k_T)$	$b(k_T)$
0.00, 0.05	0.04	0.00
0.05, 0.15	0.01	0.002
0.15, 0.25	0.06	−0.006
0.25, 0.35	0.32	−0.071
0.35, 0.45	0.82	−0.246
0.45, 0.55	1.56	−0.579
0.55, 0.65	1.69	−0.651
0.65, 0.75	1.49	−0.521
0.75, 0.85	0.27	0.395

Table 10: Coefficient a_3 for Sky Flux Equation

Latitude	a_3
5	0.50
10	0.52
15	0.55
20	0.59
30	0.63
40	0.68
50	0.72
60	0.76
70	0.80
80	0.84
85	0.86

pendix: B

Related to Geometric Mean Beam Lengths [10].

ıble 11: Geometric Mean Beam Length Ratio's and Configuration Factor for Parallel Equal Rectangular Plates

$\beta = b/c$, $\eta = a/c$, $F =$ Configuration Factor, $r =$ Geometric Mean Beam Length

η	β:	0	0.1	0.2	0.4	0.6		1.0	2.0	4.0	6.0	10.0	20.0
0	r/c	1.000	1.001	1.003	1.012	1.025		1.055	1.116	1.178	1.205	1.230	1.251
	F	—	—	—	—	—		—	—	—	—	—	—
0.1	r/c	1.001	1.002	1.004	1.013	1.026		1.056	1.117	1.179	1.207	1.234	1.255
	F		0.00316	0.00626	0.01207	0.01715		0.02492	0.03514	0.04210	0.04463	0.04671	0.04829
0.2	r/c	1.003	1.004	1.006	1.015	1.028		1.058	1.120	1.182	1.210	1.235	1.256
	F		0.00626	0.01240	0.02391	0.03398		0.04941	0.06971	0.08353	0.08859	0.09272	0.09586
0.4	r/c	1.012	1.013	1.015	1.024	1.037		1.067	1.129	1.192	1.220	1.245	1.267
	F		0.01207	0.02392	0.04614	0.06560		0.09554	0.13513	0.16219	0.17209	0.18021	0.18638
0.6	r/c	1.025	1.026	1.028	1.037	1.050		1.080	1.143	1.206	1.235	1.261	1.282
	F		0.01715	0.03398	0.06560	0.09336		0.13627	0.19341	0.23271	0.24712	0.25896	0.26795
1.0	r/c	1.055	1.056	1.058	1.067	1.080		1.110	1.175	1.242	1.272	1.300	1.324
	F		0.02492	0.04941	0.09554	0.13627		0.19982	0.28588	0.34596	0.36813	0.38638	0.40026
2.0	r/c	1.116	1.117	1.120	1.129	1.143		1.175	1.246	1.323	1.359	1.393	1.421
	F		0.03514	0.06971	0.13513	0.19342		0.28588	0.41525	0.50899	0.54421	0.57338	0.59563
4.0	r/c	1.178	1.179	1.182	1.192	1.206		1.242	1.323	1.416	1.461	1.505	1.543
	F		0.04210	0.08353	0.16219	0.23271		0.34596	0.50899	0.63204	0.67954	0.71933	0.74990
6.0	r/c	1.205	1.207	1.210	1.220	1.235		1.272	1.359	1.461	1.513	1.564	1.609
	F		0.04463	0.08859	0.17209	0.24712		0.36813	0.54421	0.67954	0.7324	0.77741	0.84713
10.0	r/c	1.230	1.232	1.235	1.245	1.261		1.300	1.393	1.505	1.564	1.624	1.680
	F		0.04671	0.09270	0.18021	0.25896		0.38638	0.57361	0.71933	0.77741	0.82699	0.86563
20.0	r/c	1.251	1.253	1.256	1.267	1.282		1.324	1.421	1.543	1.609	1.680	1.748
	F		0.04829	0.09586	0.18638	0.26795		0.40026	0.59563	0.74990	0.86563	0.95125	0.9079
∞	r/c	1.272	1.274	1.277	1.289	1.306		1.349	1.452	1.584	1.660	1.745	1.832
	F		0.04988	0.09902	0.19258	0.27698		0.41421	0.61803	0.78078	0.84713	0.90499	0.95125

R. V. Dunkle, "Geometric Mean Beam Lengths for Radiant Heat Transfer Calculations," ASME Paper No. 62–WA–120 (1962).
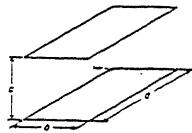
Table 12: Geometric Mean Beam Length Ratio's and Configuration Factor for Rectangular Plates at Right angles

$x = a/b$, $y = c/b$, F = Configuration Factor
$\phi = FA/b^2$, $Z_r = FAR^3/abc$, R = Geometric Mean Beam Length

x		0.05	0.10	0.20	0.4	0.6	1.0
0.02	ϕ	0.007982	0.008875	0.009323	0.009545	0.009589	0.009628
	Z_r	0.17840	0.12903	0.08298	0.04995	0.03587	0.02291
0.05	ϕ	0.014269	0.018601	0.02117	0.02243	0.02279	0.02304
	Z_r	0.21146	0.18756	0.13834	0.08953	0.06627	0.04372
0.10	ϕ		0.02819	0.03622	0.04086	0.04229	0.04325
	Z_r		0.20379	0.17742	0.12737	0.09795	0.06659
0.20	ϕ			0.05421	0.06859	0.07377	0.07744
	Z_r			0.18854	0.15900	0.13028	0.09337
0.40	ϕ				0.10013	0.114254	0.12770
	Z_r				0.16255	0.14686	0.11517
0.60	ϕ					0.13888	0.16138
	Z_r					0.14164	0.11940
1.0	ϕ						0.20004
	Z_r						0.11121
2.0	ϕ						
	Z_r						
4.0	ϕ						
	Z_r						
6.0	ϕ						
	Z_r						
10.0	ϕ						
	Z_r						
20.0	ϕ						
	Z_r						

R. V. Dunkle, "Geometric Mean Beam Lengths for Radiant Heat Transfer Calculations,"

x		2.0	4.0	6.0	10.0	20.0	∞
0.02	ϕ	0.009648	0.009653	0.009655	0.009655	0.009655	0.009655
	Z_r	0.01263	0.006364	0.004288	0.002594	0.001305	
0.05	ϕ	0.02316	0.02320	0.02321	0.02321	0.02321	0.02321
	Z_r	0.02364	0.01234	0.008342	0.005059	0.002549	
0.10	ϕ	0.04376	0.04390	0.04393	0.04394	0.04394	0.04395
	Z_r	0.03676	0.01944	0.01384	0.008018	0.004049	
0.20	ϕ	0.07942	0.07999	0.08010	0.08015	0.08018	0.08018
	Z_r	0.05356	0.02890	0.01972	0.012047	0.006103	
0.40	ϕ	0.13514	0.13736	0.13779	0.13801	0.13811	0.13814
	Z_r	0.07088	0.03903	0.02666	0.01697	0.008642	
0.60	ϕ	0.17657	0.18143	0.18239	0.18289	0.18311	0.18315
	Z_r	0.07830	0.04467	0.03109	0.02025	0.010366	
1.0	ϕ	0.23285	0.24522	0.24783	0.24921	0.24980	0.25000
	Z_r	0.08137	0.04935	0.03502	0.02196	0.01175	
2.0	ϕ	0.29860	0.33462	0.34386	0.34916	0.35142	0.35222
	Z_r	0.07086	0.04924	0.03670	0.02401	0.01325	
4.0	ϕ		0.40544	0.43104	0.44840	0.45703	0.46020
	Z_r		0.04051	0.03284	0.02226	0.01500	
6.0	ϕ			0.46932	0.49986	0.51744	0.52368
	Z_r			0.02832	0.02132	0.01272	
10.0	ϕ				0.5502	0.5876	0.6053
	Z_r				0.01759	0.01146	
20.0	ϕ					0.6608	0.7156
	Z_r					0.008975	

ASME Paper No. 62-WA-120 (1962).

Appendix: C

Kipps and Zonen CM5 Pyranometer

SOLARIMETER
FOR OUTDOOR INSTALLATION

CM 5 - CM 6

The solarimeter base is provided with a spirit level. It should be placed in a horizontal position by means of the two levelling screws.

The solarimeter CM 5 is screwed onto the base by means of the three screws provided.
The screen is fixed by pushing the three studs into the three supports on top of the base and tightening the srews.

The instrument should be positioned in such a way that the **output cable** is pointing NORTH.

In order to avoid condensation on the inside of the glass domes the interior of the solarimeter is kept dry by means of a built-in drying cartridge.
This drying cartridge (1) can be withdrawn from the mounting after removal of the retaining screw-ring (2) as indicated in fig. 1. Upon pulling the two parts of the cartridge apart, the perforated-tube can be filled with new silicagel or other suitable drying agent.

For cleaning, the outer glass dome can be taken off as indicated in fig. 1. Upon unscrewing the retaining screw-ring (3) the glass dome (4) can simply be lifted off. In re-assembling care should be taken that the ring is screwed home very tightly.

Connection to measuring equipment

The solarimeter is provided with a two-core output cable. Black is the negative terminal and blue the positive.

If long cables are used between the solarimeter and the measuring equipment, the possible influence of the resistance of these cables should be taken into account.
In the case of measuring equipment with a high input resistance (such as the integrator CC 1) the resistance of the connecting cable can usually be neglected.

When recording meters with a low internal resistance are used, the risistance of the cables may have a considerable influence. A correction is therefore required in order to avoid faulty measuring results.

For the calibration in conjunction with the solarimeter of an indicating instrument not supplied by us, two methods can be applied as shown in figures 2 and 3 page 4.
These schemes also enable the operator to determine the eventual influence of the resistance of the connecting cables.
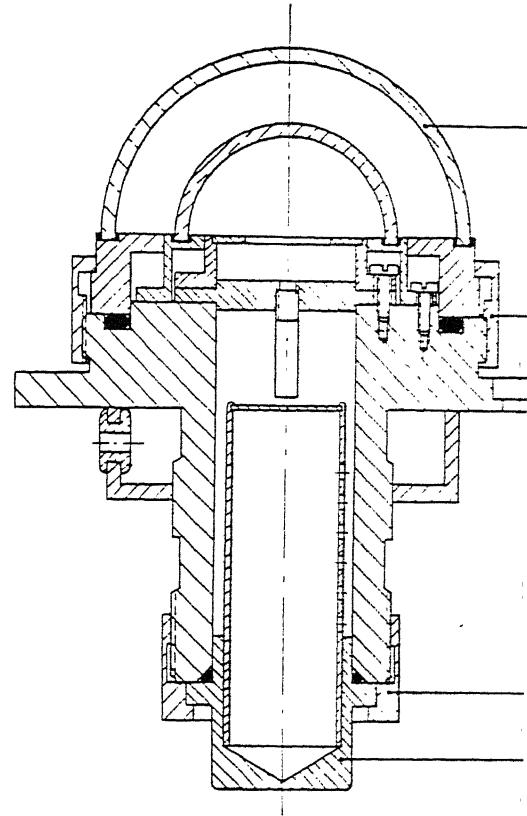
FIG. 1

Figure 36: Kipps and Zonen CM5 Pyranometer